Optical properties of the Indo-Asian haze layer over the tropical Indian Ocean

Kathleen Franke,[1] Albert Ansmann,[1] Detlef Müller,[1] Dietrich Althausen,[1] Chandra Venkataraman,[2] M. Shekar Reddy[2,3] Frank Wagner,[4] and Rinus Scheele[5]

Received 23 April 2002; revised 1 August 2002; accepted 11 August 2002; published 25 January 2003.

[1] Multiwavelength backscatter and extinction profiling was performed with a unique aerosol Raman lidar at Hulhule (4°N, 73°E), Maldives, as part of the Indian Ocean Experiment (INDOEX) between February 1999 and March 2000. The Raman lidar allowed a direct determination of the volume extinction coefficient of the particles at 355 and 532 nm at ambient conditions. Heavily polluted air masses from the Asian continent passed over the Maldives during the northeast monsoon seasons. The mean 532-nm particle optical depth was about 0.3; maximum values of 0.7 were measured. Above the polluted marine boundary layer, lofted plumes were found up to 4000-m height. On average, the free-tropospheric aerosol layers contributed 30–60% to the particle optical depth. The volume extinction coefficient at 532 nm typically ranged from 25 to 175 Mm^{-1} in the elevated layers. The pollution plumes are characterized separately for the air masses from Southeast Asia, North India, and South India. The analysis includes backward trajectories and emission inventory data for India. The extinction-to-backscatter ratio (lidar ratio) at 532 nm was mostly between 30 and 100 sr, and accumulated at 50–80 sr for highly absorbing particles from northern India. The shift of the lidar-ratio distribution for northern Indian aerosols by about 20 sr toward larger values compared to European values is consistent with an aerosol black-carbon content of up to 20%. The Ångström exponent (for short wavelengths 355/400/532 nm) ranged mostly from 1 to 1.6 for Southeast Asian particles, from 0.8 to 1.4 for North Indian pollution, and from 0.6 to 1 for South Indian air masses. The comparably low Indian Ångström exponents (indicating a comparably large mean particle radius) are possibly caused by the high contribution of biomass combustion to the aerosol formation in India. Results of a correlation analysis based on the lidar ratio, extinction coefficient, Ångström exponents, and relative humidity are presented. In most cases only a weak relationship or no relationship was found between the different parameters. *INDEX TERMS:* 0305 Atmospheric Composition and Structure: Aerosols and particles (0345, 4801); 0345 Atmospheric Composition and Structure: Pollution—urban and regional (0305); 0368 Atmospheric Composition and Structure: Troposphere—constituent transport and chemistry; *KEYWORDS:* INDOEX, lidar, aerosol remote sensing, Asian pollution, lidar ratio, particle extinction coefficient

Citation: Franke, K., A. Ansmann, D. Müller, D. Althausen, C. Venkataraman, M. S. Reddy, F. Wagner, and R. Scheele, Optical properties of the Indo-Asian haze layer over the tropical Indian Ocean, *J. Geophys. Res.*, *108*(D2), 4059, doi:10.1029/2002JD002473, 2003.

1. Introduction

[2] The tropical Indian Ocean is probably the only place in the world where an intense source of anthropogenic pollution from the Northern Hemisphere is directly connected to the pristine air of the Southern Hemisphere by a cross-equatorial monsoonal flow [*Crutzen and Ramanathan*, 2001]. For this reason, the Indian Ocean west and south of the Indian subcontinent (10°N to 17°S, 55°E to 75°E) was selected as the main field site of the Indian Ocean Experiment (INDOEX) in which several satellites, aircraft, ships, and ground stations were involved. The Intensive Field Phase (IFP) took place from January through March of 1999. Main subjects were (1) to document and characterize the Indo-Asian haze, which spreads every year, from December to April, over most of the North Indian Ocean and South and Southeast Asia, and (2) to assess the significance of the haze particles consisting of sulfates, soot, and other continental aerosols for global radiative forcing [*Ramanathan et al.*, 2001a, 2001b]. Special empha-

[1]Institute for Tropospheric Research, Leipzig, Germany.
[2]Centre for Environmental Science and Engineering, Indian Institute of Technology, Bombay, India.
[3]Now at Laboratoire d'Optique Atmosphérique, Centre National de la Recherche Scientifique, Université des Sciences et Technologies de Lille 1, Villeneuve d'Ascq, France.
[4]Meteorological Institute, University of Munich, Munich, Germany.
[5]Koninklijk Nederlands Meteorologisch Instituut, De Bilt, Netherlands.

0148-0227/03/2002JD002473$09.00

sis was put on the question: Can the haze spread to remote regions and influence the ocean heat budget and the planetary albedo (clear and cloudy) thousands of kilometers away from the source of the pollution [*Crutzen and Ramanathan*, 2001]?

[3] Aerosol plumes from India were of particular interest because of the high contribution of biomass combustion to the aerosol loading in India. The ratio of biomass-to-fossil-fuel combustion (on an energy basis) for India was estimated at approximately one in 1990–1991 [*Streets and Waldhoff*, 1998] and 0.82 in 1996–1997 [*Reddy and Venkataraman*, 2002b] and thus much larger than the average value of about 1/3 for Asia [*Streets and Waldhoff*, 1998]. Consumption of biofuels (fuelwood, crop waste, dung cake) and accidental and controlled forest and agricultural fires are the major sources of black carbon (BC, 72% of the total in India) [*Reddy and Venkataraman*, 2002b], which is the most relevant light-absorbing aerosol component in the atmosphere. Fossil fuel combustion, on the other hand, is the major contributor to the anthropogenic sulfate aerosol loading. About 95% of the emitted SO_2 in India results from fossil fuel combustion [*Reddy and Venkataraman*, 2002a]. Sulfate aerosols lead, on a global scale, to a cooling of the atmosphere whereas BC causes a warming of air masses. This warming may, in turn, have a significant impact on the atmospheric stability, the convective moisture transport, and cloud formation [*Ackerman et al.*, 2000; *Ramanathan et al.*, 2001b].

[4] The light-absorption/scattering characteristics of the particles together with their vertical distribution are most important aerosol parameters in radiative transfer calculations [*Haywood and Shine*, 1997; *Quijano et al.*, 2000a; *Wagner et al.*, 2001; *Podgorny and Ramanathan*, 2001] and must therefore be known accurately for a realistic description of aerosols in atmospheric models. Ignoring the vertical layering of aerosols can also lead to severe uncertainties in aerosol remote sensing from space [*Quijano et al.*, 2000b]. In this context it is interesting to note that the vertical distribution of aerosol properties is widely ignored in present observational and modeling efforts concerning the aerosol-climate-impact issue (Global Aerosol Climatology Project special issue in Journal of Atmospheric Science, 59(3), 2002). State-of-the-art atmospheric models are not able to reproduce adequately the vertical characteristics of the pollution outbreaks over the Indian Ocean [*Collins et al.*, 2001; *Rasch et al.*, 2001].

[5] In the following, we summarize the observations of the optical properties of the particles made by the Malé lidar station of INDOEX. We deployed a unique six-wavelength lidar, a Sun photometer, and a radiosonde station at the Malé International Airport, situated in Hulhule Island (hereafter referred to as Hulule; 4.1°N, 73.3°E), Republic of Maldives, from January 20, 1999 to April 2, 2000. Five lidars were involved in INDOEX to characterize the vertical aerosol layering. So-called micropulse lidars permitted a continuous monitoring of particle backscattering onboard the research vessel Ron Brown and at the Kaashidhoo Climate Observatory (KCO) about 80 km north of Hulule [*Welton et al.*, 2002]. Two lidars on board the National Center for Atmospheric Research C-130 and the French Mystère 20 research aircraft [*Pelon et al.*, 2002] provided detailed backscatter information regarding the spread of the pollution over the ocean.

[6] For the first time, a complex aerosol lidar was operated in the tropics to measure the optical and microphysical properties of the polluted boundary layer and lower free troposphere vertically resolved and, what is most important, under ambient conditions. Our multiwavelength lidar allowed a direct determination of the volume extinction coefficient of the particles. In the case of alternative approaches (ground-based and airborne in-situ aerosol characterizations), the scattering and absorption properties of dried aerosol particles were measured and the extinction coefficient for ambient conditions was then constructed from these two quantities [*Masonis et al.*, 2002]. A part of the particles with diameters larger than a few micrometers was not sampled due to size limitations of the aircraft inlet system. This effect can lead to a significant underestimation of the scattering properties in marine environments.

[7] Besides the determination of particle extinction-coefficient profiles at the wavelengths of 355 and 532 nm, the advanced aerosol lidar allows the simultaneous profiling of the particle 180°-backscatter coefficient at six wavelengths between 355 and 1064 nm, the extinction-to-backscatter ratio (lidar ratio) of the particles at 355 and 532 nm, the depolarization ratio at 710 nm, and the water-vapor-to-dry-air mixing ratio [*Althausen et al.*, 2000]. In contrast to Sun photometry, a clear separation of the light-extinction properties of the lofted pollution plumes from the effects caused by the marine boundary layer is possible with this lidar. From the set of the optical data, surface-area and volume concentrations, the surface-area-weighted mean radius (effective radius), and the real and imaginary part of the refractive index can be retrieved with an inversion scheme developed by *Müller et al.* [1999]. From the estimated volume size distribution and refractive index characteristics, the absorption/scattering ratio or the well-known single scattering albedo (ratio of the scattering to the extinction coefficient) of the particles can be estimated [*Müller et al.*, 2000]. The inversion results will be presented in a separate paper.

[8] Three campaigns in February/March, July, and October of 1999 were conducted to resolve the seasonal cycle of the aerosol conditions over the tropical Indian Ocean and to contrast the Indo-Asian haze observations in February/March to measurements in very clean air originating from oceanic regions of the southern hemisphere. A fourth campaign in March of 2000 was undertaken to improve the statistical significance of the observations made during the INDOEX IFP one year before. A first overview of our INDOEX activities was presented by *Müller et al.* [2001a, 2001b]. A first case study was discussed by *Ansmann et al.* [2000] (optical properties), *Müller et al.* [2000] (physical properties, single-scattering albedo), and *Wagner et al.* [2001] (radiative impact of the particles) emphasizing the most striking feature observed during INDOEX, namely that the continental pollution was mainly transported above the shallow marine boundary layer. *Franke et al.* [2001] already summarized the INDOEX results for the extinction-to-backscatter ratio.

[9] The paper contains the following sections. After a brief description of the instruments and the data analysis methods in sections 2 and 3, respectively, the observations are presented in section 4 in form of case studies, a comprehensive height- and air-mass-dependent statistical analysis of the optical properties, and correlation studies. Conclusions are given in section 5.

2. Instrumentation

[10] The containerized multiwavelength lidar is described in detail by *Althausen et al.* [2000]. Two Nd:YAG and two dye lasers emit pulses at 355, 400, 532, 710, 800, and 1064 nm simultaneously with a repetition rate of 30 Hz. The six laser beams are aligned onto one optical axis. A scanning unit outside the container permits measurements from $-90°$ to $90°$ zenith angle. Observations were typically made at zenith angles of 5, $30°$, and $60°$ during INDOEX. The lidar results presented below are given as a function of height.

[11] Backscattered light is collected with a 0.53-m Cassegrain telescope. An 11-channel receiver separates the elastically backscattered light at the laser wavelengths and the Raman signals of nitrogen at 387 nm (355-nm primary wavelength) and 607 nm (532-nm primary wavelength) and of water vapor at 660 nm by the use of dichroic beamsplitters and narrow-band interference filters. At 710 nm, the co- and cross-polarized components of the backscattered light are measured. Photomultiplier tubes (PMTs) were used as detectors at all wavelengths. For the elastic backscatter signals the analog PMT output was preamplified and digitized (12 bit, 10 MHz), whereas the Raman signals and part of the corresponding elastically scattered light at the primary wavelengths of 355 and 532 nm were detected with photon-counting PMTs operated at 300 MHz. The raw signals are stored with range and time resolution of 15–60 m and 30 s, respectively.

[12] The Sun tracking photometer SP1A05 was developed and manufactured by Dr. Schulz & Partner GmbH (Buckow, Germany). The instrument detects atmospheric attenuation of direct solar radiation in 18 calibrated channels from 351–1063 nm, from which the particle optical depth (related to the vertical column) at eight wavelengths was determined [*Wagner et al.*, 2001]. The spectral intervals (3–10 nm half width at half maximum) were selected with interference filters. The photometer was calibrated on the Zugspitze Mountain (Germany) in May of 1997 and in October of 2000. The uncertainty in the determined particle optical-depth values is 0.005–0.01 for wavelengths from 400–900 nm. These wavelengths (413, 440, 500, 530, 779, 855 nm) were most reliable during INDOEX.

[13] The Vaisala-RS-80 sonde was used to measure profiles of pressure, temperature, and relative humidity. One to four sondes per day were launched. About 250 radiosondes were released during the four field campaigns in the framework of INDOEX.

3. Lidar Data Analysis

[14] The comprehensive analysis scheme applied to the INDOEX data is similar to the one used for the analysis of observations performed during the second Aerosol Characterization Experiment (ACE 2) [*Ansmann et al.*, 2002]. Here, only a brief summary is given.

3.1. Extinction Coefficient

[15] The profiles of the volume extinction coefficient of the particles at 355 and 532 nm are calculated from the measured profiles of the nitrogen Raman signals at 387 and 607 nm, respectively [*Ansmann et al.*, 1990, 2001]. Signal averaging of 30–120 minutes and smoothing of 300–600 m in the lower and central parts of the pollution plumes (below about 2.5–3 km height) and up to 1200 m at the top of the pollution layer was necessary to reduce the statistical error of the extinction coefficient to values of the order of 5–25%. The generally low signal-to-noise ratios allowed Raman measurements throughout the troposphere only at nighttime. Signal profiles indicating clouds were removed before averaging.

[16] The extinction measurements were biased by the incomplete overlap of the laser beam and the receiver field of view below 3 km height. However, during clear and less-polluted nights the overlap profile of the lidar could be determined by applying the procedure suggested by *Wandinger and Ansmann* [2002]. The deviations between the different overlap profiles measured in February, March, July, and October of 1999, and in March of 2000 were small. By considering these different overlap profiles in the extinction calculations the resulting absolute error (standard deviation) in the extinction values was estimated to be about 25 Mm^{-1} at 1-km height and 15–20 Mm^{-1} for heights $\geq$1.5 km [*Franke*, 2003]. For distances <1 km a trustworthy retrieval of the extinction profile was not possible because of the large overlap correction uncertainties.

[17] Systematic errors are also introduced by correction for molecular effects [*Ansmann et al.*, 1992; *Ferrare et al.*, 1998; *Masonis et al.*, 2002]. Several radiosonde launches per day at the field site provided actual pressure and temperature profiles to determine the needed Rayleigh extinction and nitrogen number-density profiles. The overall relative systematic error is about 30–50% for low extinction coefficients around 30 Mm^{-1} and <15% for extinction coefficients $\geq$100 Mm^{-1}.

[18] The mean particle extinction coefficient at 532 nm for the lowermost 1000 m was estimated by comparing the 530-nm particle optical depth derived from Sun photometer observations about one hour before sunset with the lidar-derived 532-nm particle optical depth for the vertical tropospheric column >1000-m height. The lidar observations were conducted typically 0.5–3 hours after sunset. The uncertainty in the mean extinction coefficient for the lowermost 1000-m height includes the uncertainties in the lidar- and Sun-photometer-derived values and an estimated 20% uncertainty accounting for possible temporal changes of the optical depth from the afternoon hours to the lidar measurement hours.

3.2. The 180° Backscatter Coefficient

[19] The profiles of the volume backscatter coefficients at 355 and 532 nm were determined from the profiles of the ratio of the elastic backscatter signal (355, 532 nm) and the corresponding nitrogen Raman signal (387, 607 nm) [*Cooney et al.*, 1969; *Melfi*, 1972; *Ansmann et al.*, 1992]. The same temporal averaging is applied as for the extinction

analysis. Signal smoothing of 180 m is sufficient to reduce the relative error induced by signal noise to <10%. The overlap effect does not play a role because the determination is based on signal ratios so that the overlap effect cancels out.

[20] In order to calibrate the signal ratio profile, a region in the free troposphere with negligible particle backscattering (Rayleigh calibration) is needed. Such a region was always available, typically in the 6–10-km height range. Again, air density (radiosonde) information is used for the removal of Rayleigh scattering and backscattering effects on the signal ratios. Both, the relative systematic and the statistical errors of the particle backscatter coefficient are 5–10%.

[21] The particle backscatter coefficients at 400, 710, 800, and 1064 nm must be calculated from the elastic backscatter signals alone because reference Raman signals are not available. The so-called Klett method [*Klett*, 1981] is applied here. We used the formalism basically developed by *Fernald* [1984] in the version presented by *Sasano et al.* [1985]. The procedure considers a wavelength-dependent lidar ratio [after *Ackermann*, 1998] and assumes that the vertical distribution of the lidar ratio at the above mentioned wavelengths is the same as the one determined for 532 nm. Signal calibration is also needed here and is done as described above. Because in most observational cases a cirrus deck was present the quality of the calibration could be checked by assuming wavelength-independent backscattering by ice crystals. The data analysis is described in detail by *Ansmann et al.* [2002].

[22] As in the case of the extinction coefficient calculation, the overlap effect has to be corrected for before applying the Klett method. The uncertainty of the correction does not allow a trustworthy determination at distances <1000 m from the lidar. The statistical error of particle backscatter coefficients determined from elastic backscatter signals with the Klett method is 5–10%. The systematic errors are estimated to be 10–20% [*Ansmann et al.*, 2002].

3.3. Lidar Ratio

[23] Before calculating the lidar ratios at 355 and 532 nm the extinction and backscatter coefficients were determined from signal profiles smoothed with window lengths of 180 m. Then, the resulting lidar-ratio profile was further smoothed with 600-m window length. The overall error of the lidar ratio typically ranges between about 20% and 30% in the lofted pollution plumes.

3.4. Ångström Exponent

[24] From the spectrally resolved backscatter and extinction coefficients, profiles of the Ångström exponent can be calculated. The Ångström exponent $å$ [*Ångström*, 1961] is the most commonly used atmospheric spectral aerosol index. If observations are made in aerosols that consist of accumulation-mode particles (diameters <1 μm, anthropogenic particles) and coarse-mode particles (diameter >1 μm, large marine particles), the use of two Ångström exponents, one for short wavelengths (≤532 nm, sensitive to small particles with diameters ≤ 0.2 μm) and one for the longer wavelengths (sensitive to larger-sized particles), may be of advantage [*Reid et al.*, 1999; *Ansmann et al.*, 2002].

[25] The Ångström exponent for the particle extinction coefficient σ_λ is defined as

$$å_{\lambda_1,\lambda_2}(z) = -\frac{\ln[\sigma_{\lambda_1}(z)/\sigma_{\lambda_2}(z)]}{\ln(\lambda_1/\lambda_2)}. \quad (1)$$

In the case of the Raman-lidar solution for the extinction coefficient $\sigma_\lambda(z)$, $\lambda_1 = 355$ nm and $\lambda_2 = 532$ nm.

[26] If backscatter coefficients β_λ together with lidar ratios S_λ are used, we obtain [*Ansmann et al.*, 2002]

$$å_{\lambda_1,\lambda_2}(z) = -\frac{\ln\{[S_{\lambda_1}(z)\beta_{\lambda_1}(z)]/[S_{\lambda_2}(z)\beta_{\lambda_2}(z)]\}}{\ln(\lambda_1/\lambda_2)}. \quad (2)$$

The uncertainty in $å$ after equation (2) is large if the wavelength dependence of the lidar ratio is not known as it is the case for the 532–1064-nm wavelength range. The wavelength dependence in the short-wavelength range is usually known from the Raman lidar observations. The wavelength dependence of the lidar ratio for anthropogenic aerosols as suggested by *Ackermann* [1998] (compare Figure 4 of *Ansmann et al.* [2002]) is assumed in the INDOEX data analysis.

[27] In the next section, mostly values for $å_{400,532}$ for the 400–532-nm wavelength range and $å_{532,800}$ for the 532–800-nm wavelength range are presented. These Ångström exponents were chosen because they are most appropriate for comparisons with respective values derived from Sun photometer observations (400–900-nm spectrum) and with ACE-2 values. During ACE 2, most of the time only the lidar wavelengths from 400–800 nm were available. In a few cases in March 2000 the wavelengths of 355, 532, and 710 nm had to be used to calculate the Ångström exponents. Because of a severe laser damage the 400 and 800-nm lidar signals were then not available. The quality of the Ångström values $å_{355,532}$ and $å_{400,532}$ calculated from the backscatter coefficients were checked by comparison with respective exponents directly determined from the 355 and 532-nm extinction profiles. Errors of the Ångström values for the short and the long wavelengths calculated from the backscatter coefficients are estimated to be of the order of 20–30% and 20–40%, respectively [*Ansmann et al.*, 2002].

3.5. Relative Humidity

[28] The ratio of the water-vapor Raman signal to the nitrogen Raman signal yields the water-vapor-to-dry-air mixing ratio [*Melfi et al.*, 1969; *Ansmann et al.*, 1992]. By using the temperature information of a radiosonde ascent at the lidar site the relative humidity is estimated. Relative errors in the lidar-derived water-vapor mixing ratios are about 5–20% depending on temporal averaging of lidar profiles, signal smoothing length, distance from the lidar (height), and amount of detected water vapor. The same temporal averaging as in the case of the backscatter and extinction calculation was applied to investigate the influence of the relative humidity (measured in the same air volume) on the particle optical properties.

4. Observations

4.1. Case Studies

[29] Backward trajectories showed that anthropogenic aerosols were mainly advected from Southeast Asia (Indo-

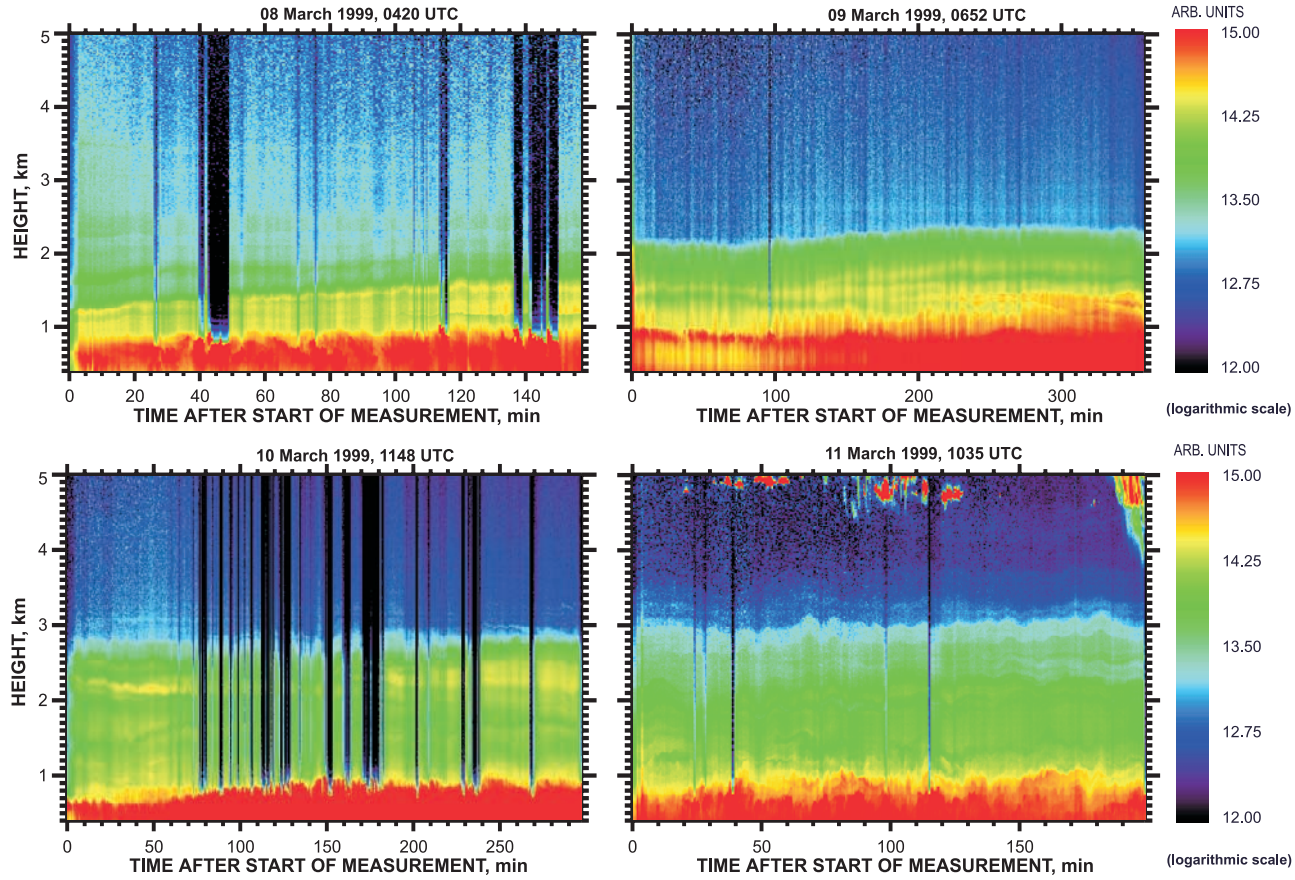

Figure 1. Time-height display of the range-corrected 532-nm backscatter signal on four subsequent days (March 8–11, 1999) during the buildup of an Indian pollution plume. Start times of the measurements are indicated above each of the plots; the observational periods lasted between three and six hours. Red indicates the convective boundary layer, and yellow and green indicate the lofted aerosol layers. The column-like structures are caused by dense cumulus clouds (black) and by the variable laser output energy resulting from the continuously varying electric power on the airport, especially on March 9.

china, East Asia, Philippines) during the first phase of the INDOEX IFP. During the second phase, beginning on March 9, 1999, most of the air masses observed over Hulule originated from northern India. In March 2000, anthropogenic aerosol particles originated from South India (before March 18) and North India (March 19–23).

[30] Figure 1 illustrates the buildup of the Indian pollution plume observed from March 8–11, 1999. *Pelon et al.* [2002] conducted airborne lidar observations during this pollution outbreak between Hulule and about 500–700 km northwest and southeast of Hulule. The pronounced layer below 1000-m height (in red in Figure 1) indicates the convective marine boundary layer, which typically reached into heights of 500–900 m in February and March of 1999 [*Franke*, 2003]. According to backward trajectories shown in Figure 2 for an arrival height of 2 km above Hulule, pollution layers from Southeast Asia were still present in the free troposphere above the Maldives on March 8, 1999. The trajectory model [*Scheele et al.*, 1996] used 3-dimensional wind vectors and temperatures that were obtained from the operational (T213) model of the European Centre for Medium-Range Weather Forecasts.

[31] The lofted layers observed in the following days (March 9–11, 1999) originated from northern parts of India. These air masses crossed the Bay of Bengale with the prevailing northeasterly trade winds and traveled about 6 days after leaving northern India before they reached the lidar site. Our Sun photometer observed a steady increase of the 500-nm optical depth from 0.2–0.3 on March 8, 1999, to values of 0.6–0.7 on March 11, 1999. The Ångström exponent, calculated from the optical depths measured at 413 and 530 nm, increased from 0.7 on March 8, 1999, to 1.1 on March 11, 1999.

[32] The main reason for the observed layering is believed to be the lifting of the continental air above the colder oceanic air (marine boundary layer) when the pollution plumes are advected across the coastline [*Angevine et al.*, 1996; *Ansmann et al.*, 2001]. The resulting air transport pattern may have been modulated by sea breeze effects [*Léon et al.*, 2001; *Pelon et al.*, 2002].

[33] Vertical profiles of the particle backscatter and extinction coefficients, of the lidar ratios, and of the Ångström exponents taken after sunset on March 10 (compare Figure 1, 1450–1650 UTC) are presented in Figure 3. Figure 4 shows the radiosonde profiles of potential temperature and relative humidity, measured between 1618 and 1640 UTC on that day together with the relative humidity derived from the lidar observations. Backward trajectories

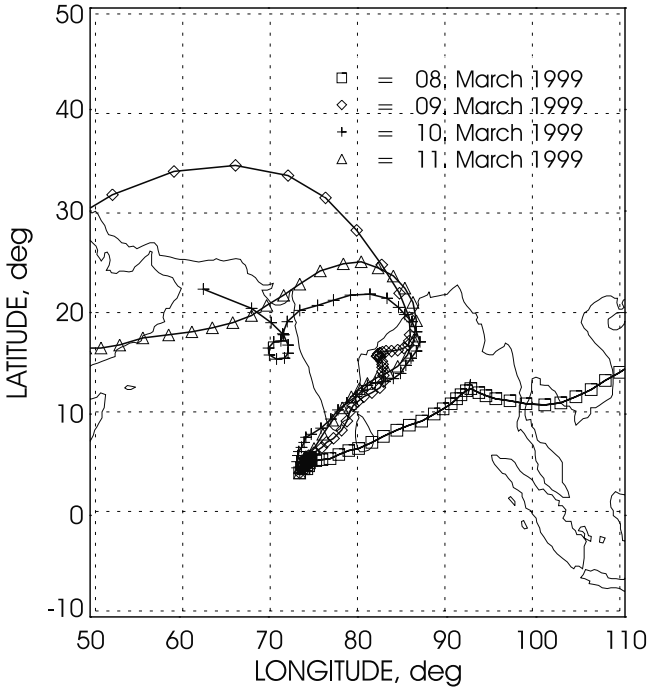

Figure 2. Ten-day backward trajectories for the arrival height of 2000 m (compare Figure 1) over Hulule. Arrival times are 0600 UTC (March 8, 1100 local time), 1000 UTC (March 9), 1500 UTC (March 10), and 1100 UTC (March 11). The time step between individual symbols is 4 hours.

for the center of the marine boundary layer (500-m height), for the transition layer (1500 m), and for the center of the pollution layer (2300 m) are given in Figure 5.

[34] As can be seen, above the marine boundary layer a heavily polluted continental layer with maximum volume extinction coefficients of 200 Mm^{-1} at 532 nm was present. According to the radiosonde observations, the boundary layer is characterized by an increasing relative humidity and the almost height-independent potential temperature below 800 m (compare Figure 4). The extremely large backscattering coefficients in the lowermost 250 m result from light scattering by moist large sea-salt particles. This feature was observed in about 90% of the INDOEX IFP measurements.

[35] The air mass, which arrived at Hulule around 1500-m height crossed predominantly less populated regions mostly at heights above 4.5 km (above sea level, ASL) and the southern tip of India at heights between 3 and 4 km ASL. This may explain the low backscatter and extinction coefficients around 1500-m height. The 2300-m-height backward trajectory in Figure 5 indicates that the pronounced free-tropospheric aerosol layer originated from the polluted Indian subcontinent. The air mass crossed central India with relatively low wind speed at heights of 3.5–5.5 km ASL (about 3–5 km above ground level, AGL) and the southern tip of India at heights of 2–3 km ASL (about 1.5–2.5 km AGL).

[36] The stable stratification above the convective boundary layer indicated by the increasing potential temperature with height (compare Figure 4) prohibited mixing between the marine and the continental aerosol layers. The relative humidity was below 65% in the lofted pollution layer so that it is most likely that the particles were dry. The optical depths for the columns below and above 1000-m height were 0.16 and 0.26 at 532 nm, respectively. In the calculation it was assumed that the total particle optical depth was 0.42 as measured with Sun photometer about 2 hours before the lidar measurement. The free troposphere thus contributed about 60% to the total particle optical depth.

[37] The extinction-to-backscatter ratios in Figure 3 were found to be equal at both lidar wavelengths in the lofted pollution plume. Values between 50 and 75 sr are typical for polluted air [*Ansmann et al.*, 2001; *Ferrare et al.*, 2001]. The 532-nm lidar ratio for the lowermost 1000 m of about 35 sr indicates a mixture of marine and anthropogenic particles. Marine particles typically cause lidar-ratio values below 30 sr [*Ansmann et al.*, 2001; *Franke et al.*, 2001].

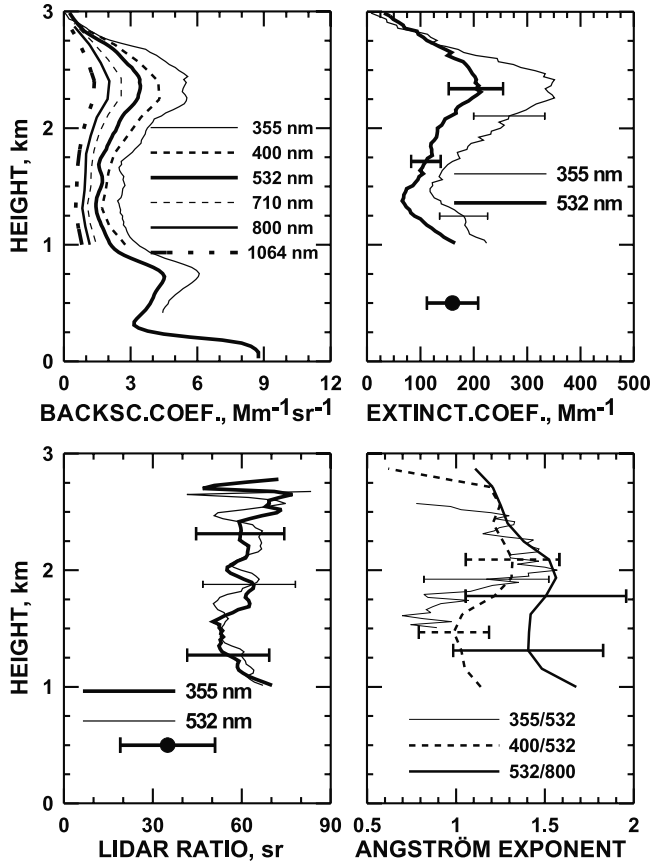

Figure 3. Two-hour average profiles of the particle backscatter coefficient at the six emitted laser wavelengths, of the extinction coefficient and the lidar ratio for two wavelengths, and of the Ångström exponent for three different wavelength pairs as determined from the multi-wavelength observation on March 10, 1999, 1457–1700 UTC. Signal files containing cloud signatures were removed before averaging. $å_{400,532}$ and $å_{532,800}$ are calculated from backscatter coefficients, and $å_{355,532}$ is calculated from extinction coefficients. The average extinction and lidar-ratio values for the lowermost 1000 m (solid circles) are derived by combining Sun photometer (total column) and lidar observations (column for heights >1000 m). Error bars indicate the standard deviation accounting for systematic (retrieval) errors and signal noise.

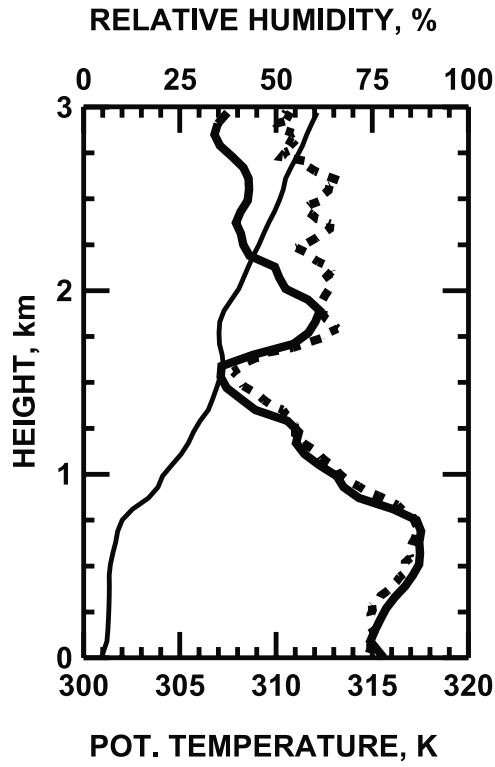

Figure 4. Observation of potential temperature (thin solid line) and relative humidity with radiosonde (thick solid line) launched on March 10, 1999, 1618 UTC. The two-hour average profile of the relative humidity derived from the lidar observation (dashed line) on March 10, 1999, 1457–1700 UTC, is shown for comparison.

The lidar ratio for the lowest 1000 m was calculated from the shown mean extinction coefficient and the backscatter coefficient integrated from the surface to 1000-m height.

[38] The Ångström exponents were 1–1.5 in the upper part of the pollution layer. Good agreement was found between the different Ångström values for the short-wavelength region calculated from the backscatter and extinction coefficients. The comparably large deviations between the exponents for the shorter wavelengths and $å_{532,800}$ around 1500-m height may be caused by the large uncertainties in $å_{532,800}$ of 20–40%. However, the observed height profiles of $å_{400,532}$ and $å_{532,800}$ are consistent with an almost height-independent influence of larger-sized particles on light scattering whereas the influence of pollution particles (diameters <0.2 μm) was low in the descending air mass observed at 1500-m height and high in the pronounced plume above 2000-m height. The Sun photometer measurements, made several hours before, support the lidar observations. The column-mean values $å_{413,530}$ and $å_{530,779}$ were 1.2 and 1.5, respectively.

[39] As mentioned above, three advection patterns determined the airflow during the INDOEX IFP and the March-2000 campaign. Figure 6 shows one example for each of the defined clusters. The clusters were chosen similar to the ones shown by *Franke et al.* [2001]. Cluster 1 (Southeast Asia) includes all backward trajectories from Southeast Asia which never were over the Indian subcontinent or crossed only the southernmost part of India before ending at Hulule (compare Figure 6, March 2, 1999). Cluster 2 (North India) includes all cases with air masses which crossed northern India and traveled out over the Bay of Bengale north of 16.2°N (compare Figure 6, March 24, 1999). These air masses traveled, on average, 4–6 days after leaving northern India and before arriving at Hulule. The third cluster (South India) contains the remaining backward trajectories which mostly crossed southern India (compare Figure 6, March 17, 2000).

[40] Relatively large lidar ratios (60–90 sr) were frequently observed in northern Indian plumes indicating light-absorbing particles [*Franke et al.*, 2001]. Slightly lower lidar ratios around 50 sr were typical for the Southeast Asia cluster. The lowest lidar ratios were observed when the lofted pollution plumes crossed South India. The 355-nm lidar ratios were, on average for INDOEX, about 10% larger than the 532-nm values. According to the Ångström exponents of roughly 0.8–1.2 for Indian pollution and 1.2–2 for Southeast Asian aerosols, Indian particles were obviously larger than Southeast Asian aerosol particles. Possible reasons are (1) differences in the removal of large particles by, e.g., precipitation along the different transport ways from India and from Southeast Asia to the Maldives, (2) differences in the strength of small-scale and mesoscale convective lifting along the two different ways upwind of Hulule leading to the injection of large marine particles into the free troposphere, (3) a significant contribution of soil dust particles in the Indian air masses, and (4) a larger fraction of large biomass-burning particles in the Indian pollution plumes. The influence of the latter effect (effect 4) is discussed in more detail in the next section. Finally,

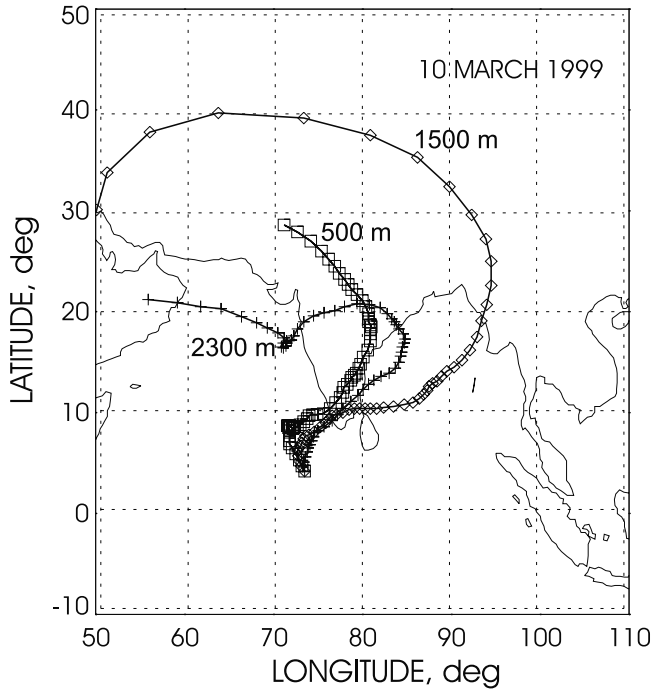

Figure 5. Ten-day backward trajectories for the arrival heights of 500 m (center of the boundary layer, compare Figure 3), 1500 m, and 2300 m (center of the lofted pollution layer). Arrival time is 1600 UTC. The time step between individual symbols is 4 hours.

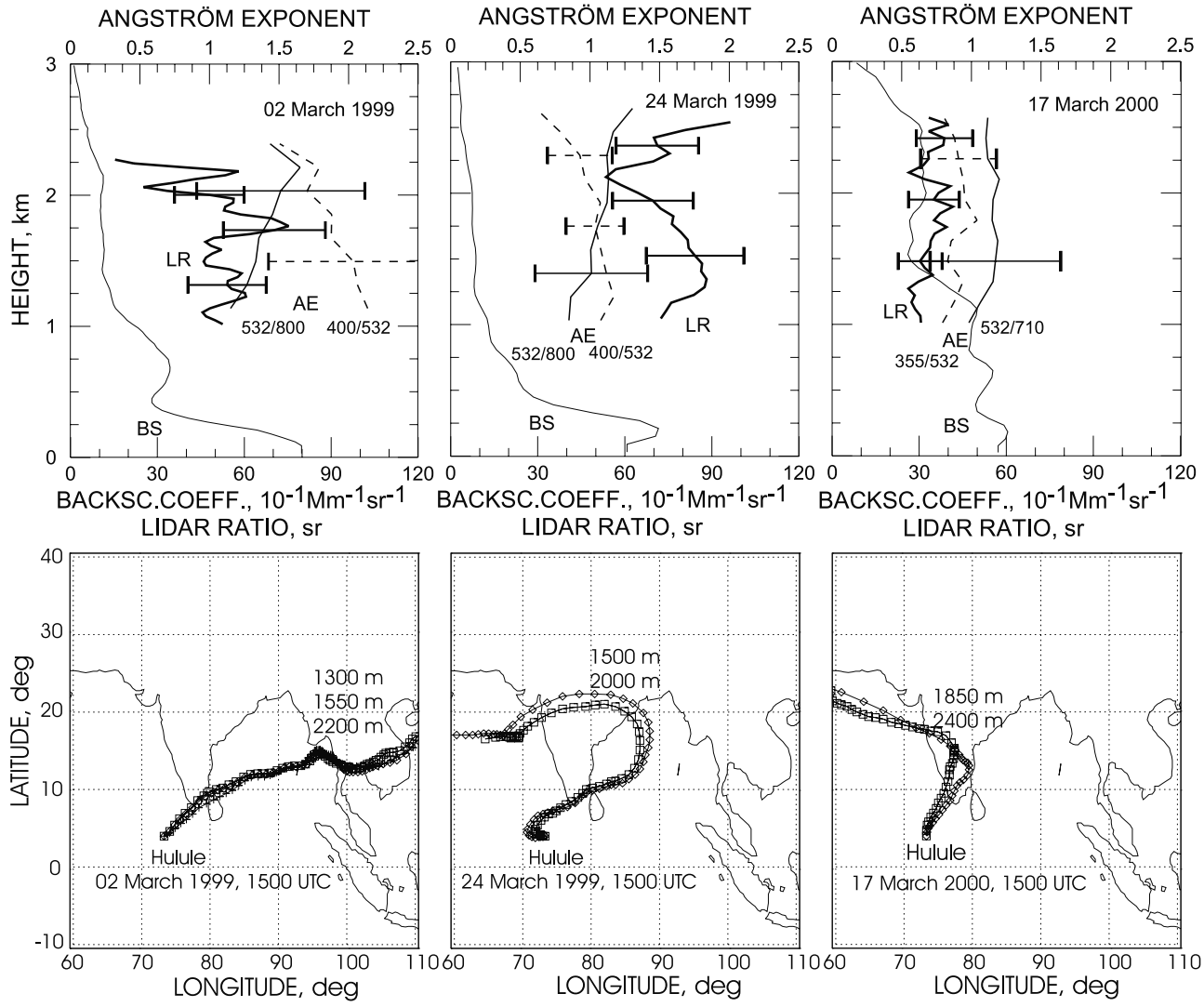

Figure 6. Lidar observations of the particle backscatter coefficient (BS, thin solid line), particle lidar ratio (LR, thick solid line), Ångström exponents $å_{400,532}$ and $å_{355,532}$ (AE, dashed line) and $å_{532,710}$ and $å_{532,800}$ (AE, solid line), and associated backward trajectories (arrival times and heights are given in the plots). The lidar measurements were made on March 2, 1999, 1456–1516 UTC, March 24, 1999, 1415–1515 UTC, and March 17, 2000, 1431–1600 UTC. They belong to the Southeast Asian cluster (left), North Indian cluster (center), and South Indian cluster (right).

differences in the aging of Southeast Asian and Indian particles may have contributed to the different Ångström exponents.

[41] Figure 7 shows the relative contribution of the lofted plumes to total light extinction as estimated from the limited set of combined photometer/lidar observations taken around sunset. To avoid confusion, the case with the maximum optical depth of 0.7 is not included because this measurement was made with Sun photometer around noon on March 11, 1999. In the evening, accurate Sun photometer observations were not possible because of low and high clouds.

[42] As can be seen, the 532-nm optical depth especially for Indian air masses (March 9–25, 1999, and March 9–23, 2000) varied around 0.3 and the pollution above 1000-m height contributed about 30–60% to the total particle optical depth. The impact of free-tropospheric particles was less pronounced for Southeast Asian air masses, i.e., before March 8, 1999. For comparison, under clean conditions in October of 1999 the particle optical depth was, on average, 0.12 ± 0.02 at 530 nm and the average contribution of the free troposphere (>1000 m) was 24%. A similar value for the marine particle optical depth was estimated from our Sun photometer observations during the INDOEX IFP [*Wagner et al.*, 2001]. If we now assume a marine optical depth of 0.1 (below 1000-m height) the contribution of the particles in the lofted layers to the total optical depth for anthropogenic particles was often as high as 60–80% during the INDOEX IFP and during March of 2000.

4.2. Air-Mass-Related Optical Properties

[43] Figure 8 summarizes the aerosol optical properties for the clusters 1–3. A fourth cluster (southern-hemispheric marine conditions) includes all trajectories which never

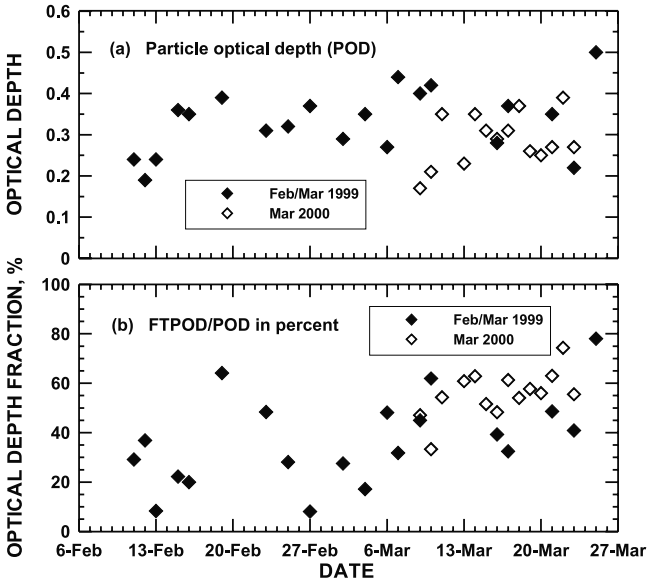

Figure 7. Particle optical depth (POD) at 532 nm and the ratio of the free-tropospheric particle optical depth (FTPOD, column above >1000-m height) to POD. The Sun photometer provided POD, and FTPOD was determined with lidar. The INDOEX IFP values are indicated by solid symbols, and the March 2000 observations are indicated by open symbols.

touched a continent during the 10 days before arrival at Hulule. This air originated from the southern hemisphere. Such observations were made in October of 1999. The optical properties in Figure 8 are mean values for four layers from 0–1000 m, 1000–1500 m, 1500–2000 m, and 2000–2500 m. Before the averaging of the individual measurement cases, backward trajectories arriving over Hulule at 950 hPa, 870 hPa, 820 hPa, and 770 hPa were used to determine to which cluster the column-mean data points for the layers from 0–1000 m, 1000–1500 m, 1500–2000 m, and 2000–2500 m, respectively, belong. The resulting cluster-related vertical distributions of optical properties for the clusters 1 and 2 in Figure 8 are very similar to the mean profiles of observations conducted during the first phase of the INDOEX IFP (before March 9, 1999) and the second phase of the IFP (beginning on March 9, 1999), respectively.

[44] The values for the lowest layer from 0–1000 m characterize the polluted marine boundary layer. According to our observations based on lidar backscatter and radiosonde potential-temperature profiling and in agreement with lidar measurements by *Welton et al.* [2002] during the cruise of the Ron Brown in the Indian Ocean between 10°S and 19°N, the marine boundary layer top height was, with only a few exceptions, below 1000 m height. The values for the three 500-m-deep layers above 1000-m height characterize the elevated continental haze plumes. However, as mentioned, it can never be excluded, especially in the tropics, that polluted marine air penetrated into the free troposphere by convective motions several hundreds to thousands of kilometers upwind of Hulule.

[45] The mean values of the particle extinction coefficient in the lowermost layer are largest as the result of strong scattering by marine and anthropogenic particles. Average extinction coefficients close to 200 Mm^{-1} were found for clusters 1 and 2. These values are about a factor of two larger than the respective marine values (cluster 4). According to this result the contribution of anthropogenic particles

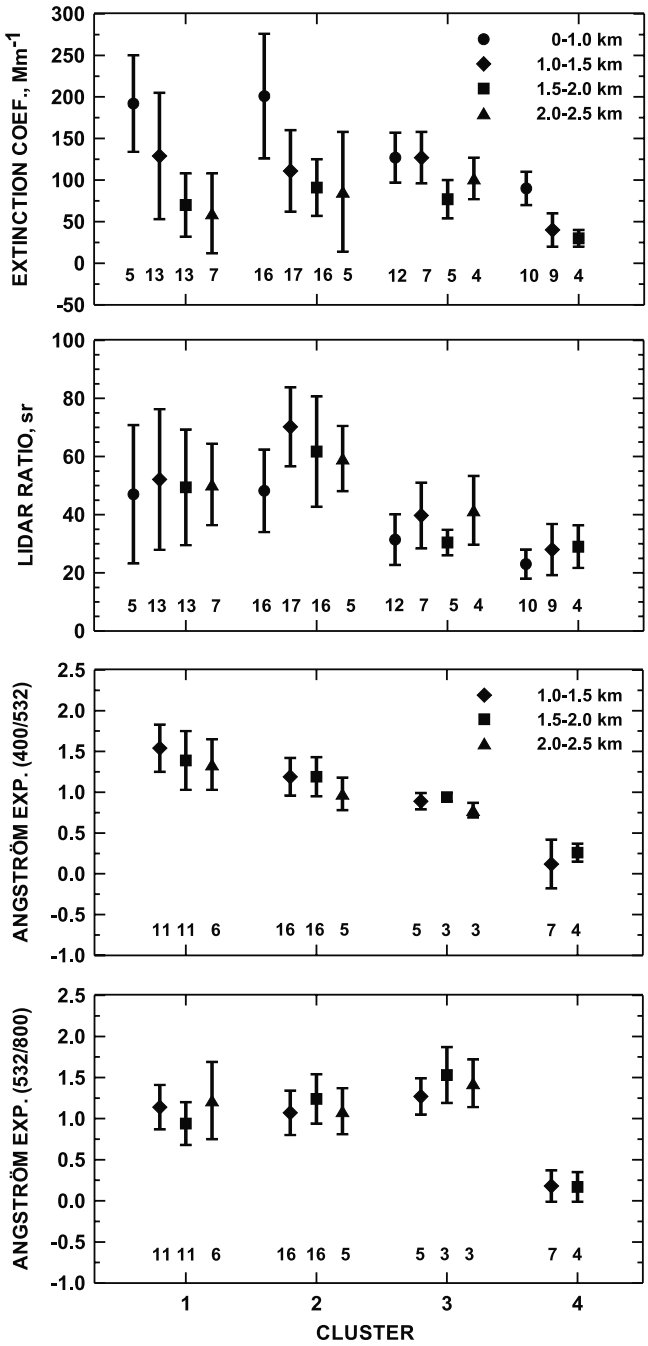

Figure 8. Cluster-mean particle extinction coefficient (532 nm), lidar ratio (532 nm), and Ångström exponents for short and long wavelengths for the height layers from 0–1000 m, 1000–1500 m, 1500–2000 m, and 2000–2500 m. Bars indicate the standard deviation. Numbers of observations for each group are given in the plots. Clusters 1–3 are the Southeast Asia (1), North India (2), and South India (3) clusters. Cluster 4 includes observations in clean marine air in October of 1999.

to light extinction was close to 50% in the marine boundary layer for clusters 1 and 2. The comparably large cluster-1 values, which were in all heights as high as the values related to the highly populated northern parts of India, imply that, in addition to Indochina, East Asia (China, Japan, Philippines) contributed strongly to the aerosol burden.

[46] In contrast to the Asian pollution plumes with typical extinction values from 25–175 Mm^{-1} above 1000-m height, European pollution-outbreak plumes observed during ACE 2 showed extinction values mostly from 30–70 Mm^{-1} at 532 nm. In only 14% of all cases the extinction coefficient in the lofted European plumes was larger than 100 Mm^{-1} [*Ansmann et al.*, 2001]. In terms of particle optical depth, European pollution outbreaks showed values from 0.15–0.25 at the Portuguese coast, whereas peak values of up to 0.7 were found over Hululе more than 3000 km south of the main anthropogenic sources. The top heights of the lofted ACE-2 pollution plumes at the Portuguese coast were mostly between 1500- and 3400-m height (2400-m mean value). The top heights of the haze layers ranged from 1900–3000 m (2600-m mean value) for Southeast Asian haze layers and 2200–4000 m (2900-m mean value) in the case of Indian aerosol plumes.

[47] On the basis of our combined photometer/lidar observations around sunset, the monthly mean particle optical depth at 530 nm was 0.31 ± 0.07 (February 1999), 0.35 ± 0.08 (March 1999), and 0.29 ± 0.05 (March 2000) [*Müller et al.*, 2001a] and agreed quite well with values of 0.32 ± 0.14 (February 1999), 0.46 ± 0.16 (March 1999), and 0.32 ± 0.11 (March 2000) at 500 nm derived from Sun photometer observations [*Eck et al.*, 2001] at KCO about 80 km north of Hululе. The March-1999 mean value at KCO is considerably larger and includes daily mean optical depths of up to 1.1. We never observed particle optical depths >0.7 at 500 nm with Sun photometer at Hululе. Our results are in agreement with continuous (24 hour per day) micropulse lidar observations at KCO. Maximum values of the optical depth at the micropulse-lidar wavelength of 523 nm did not exceed 0.75 before March 25, 1999 (last day of our observations) [*Welton et al.*, 2002]. Different cloud screening procedures applied to the lidar and photometer data sets may have caused the discrepancies.

[48] The lidar ratios presented in Figure 8 were already discussed by *Franke et al.* [2001]. It was suggested that the comparably large lidar ratios of the North India cluster, especially in the 1–1.5-km layer, were caused by strongly absorbing particles. To support this hypothesis, Figure 9 compares the trajectories for air masses above 1000-m height cases with very large lidar ratios, S > 70 sr (red trajectories), and very low, non-marine lidar ratios, S < 40 sr (yellow trajectories). The underlying map in Figure 9 shows the ratio of sulfur dioxide (SO_2) emission to black carbon (BC) emission after *Reddy and Venkataraman* [2002a, 2002b] for the INDOEX IFP period (January–March of 1999). The map may also be roughly interpreted in terms of the ammonium sulfate/BC ratio in the aerosol emission fluxes from India by assuming a SO_2-to-sulfate conversion rate of 0.6 [*Venkataraman et al.*, 1999] and by keeping in mind that the molecular weight of ammonium sulfate is a factor of 2 higher than the one of SO_2. According to the underlying emission map, aerosols from the northern and eastern parts of India have a high BC content. For these aerosols, the particle absorption-to-scattering ratio and also the lidar ratio is expected to be high. This is confirmed by Figure 9. For S > 70 sr, 17 out of 21 trajectories crossed northern India where the SO_2/BC ratio was frequently below three during January–March, 1999. Comparable pollution conditions were found during strong winter smog situations at urban sites in central Europe in the early 1980s [*Heintzenberg and Mészáros*, 1985]. For S < 40 sr, all air masses crossed southern India or arrived from Southeast Asia. In southern India the SO_2/BC ratio (or ammonium sulfate/BC ratio) typically ranges from 3–10. Similar values are valid for Thailand (main contributor in Indochina) and East Asia as can be concluded from the ratios of biomass combustion to total energy consumption [*Streets and Waldhoff*, 1998]. According to *Neusüß et al.* [2002] ammonium sulfate/BC ratios of about 3–5 are also typical for rural sites in central Europe. Shipborne measurements in the eastern Atlantic Ocean during ACE 2 yielded sulfate/BC ratios around 15, about five times higher than values found in lofted plumes off the east coast of the United states [*Novakov et al.*, 2000a].

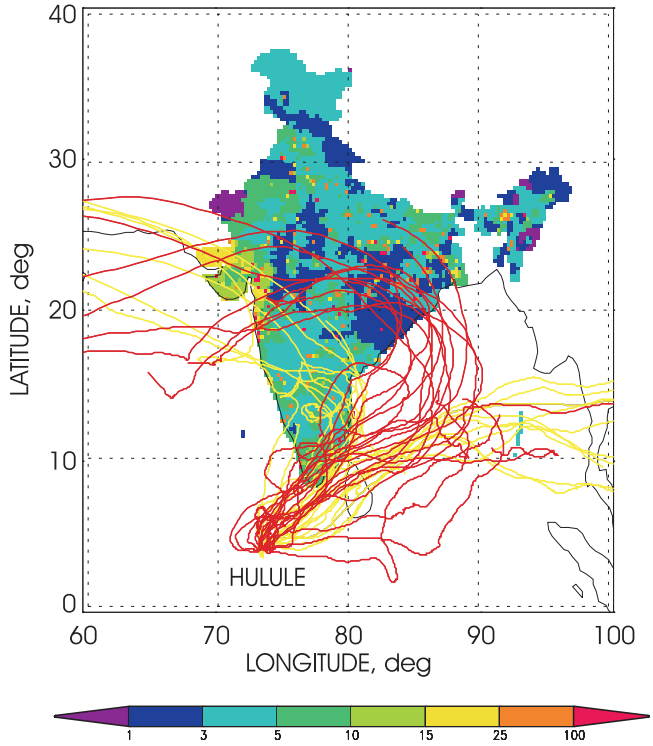

Figure 9. Geographical distribution of the ratio of SO_2 emission to BC emission (underlying map, mainly in blue and green) for the INDOEX IFP period, backward trajectories (in red) arriving at Hululе for lofted aerosols showing a high lidar ratio >70 sr (indicating highly absorbing particles), and backward trajectories (in yellow) for low lidar ratios <40 sr (indicating less absorbing particles). The red trajectories mainly crossed northeastern parts of India where large areas with low SO_2/BC ratios (blue) exist, indicating a high BC content in the aerosol.

[49] In Figure 10, the lidar ratios of the North India cluster and of ACE-2 aerosols (lofted pollution plumes [*Ansmann et al.*, 2001]) are compared. The lidar-ratio

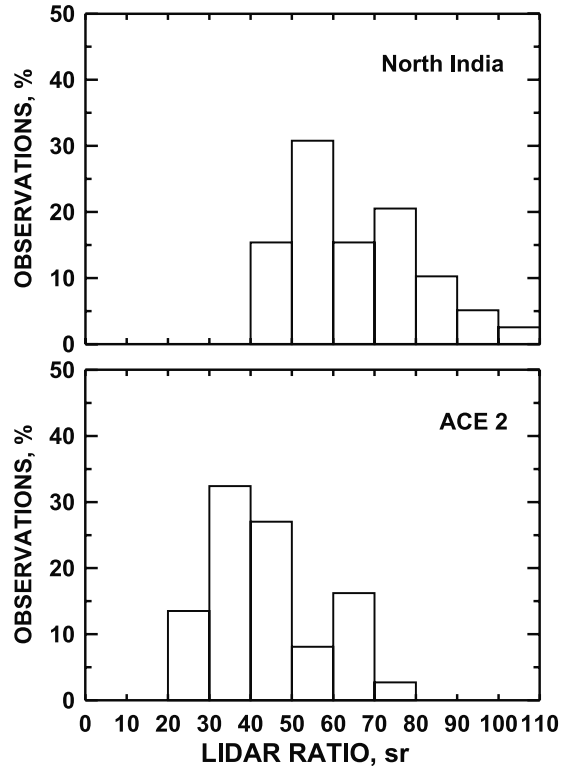

Figure 10. Distribution of the 532-nm lidar ratios of the lofted aerosol layers for the North India cluster and for ACE 2 (European pollution outbreaks).

distribution for northern Indian particles is clearly shifted toward larger values with respect to the European distribution. The shift can be largely explained by the absorption effect. If we assume, for example, (1) an externally mixed aerosol of absorbing and non-absorbing particles, (2) a mass scattering efficiency of about 4.5 m^2g^{-1} for non-absorbing particles, (3) a mass absorption efficiency of 9 m^2g^{-1} for absorbing (BC) particles [*Venkataraman et al.*, 1999; *Reddy and Venkataraman*, 2000], and (4) a scattering-to-backscattering ratio of about 40–50 sr for typical size distributions of anthropogenic particles [*Ackermann*, 1998], the respective backscatter and extinction coefficients yield lidar ratios of 45–55 sr and 65–75 sr for aerosols with a BC content of 5% and 20%, respectively. *Novakov et al.* [2000b] measured maximum BC contents of 15–20% of the fine-particle mass of the elevated Indian aerosol plumes.

[50] It should be mentioned that the lidar ratio not only depends on the chemical composition (refractive index); it is also a function of size and shape of the particles. Shape effects have to be considered in the case of backscattering by ice crystals [*Ansmann et al.*, 1992] and by desert dust particles [*Mattis et al.*, 2002], and can be ignored in the case of anthropogenic pollution particles with effective radii <0.25 μm [*Ferrare et al.*, 2001; *Wandinger et al.*, 2002]. Concerning the influence of particle size, our Mie calculations show that changes in the lidar ratio are minor even in the case of an effective radius increasing from 0.1 to 0.2 xμm. The 0.1–0.2-μm effective-radius range covers most of the INDOEX values derived from our lidar data by means of an inversion technique [*Müller et al.*, 2001b]. Our simulations were based on realistic size distributions and anthropogenic aerosol mixtures as reported by *Ackermann* [1998] and yielded a lidar ratio which was roughly constant or decreased with increasing effective radius. Only when the relative humidity increased from rather low values to close to 100%, a significant increase of the lidar ratio (by about 20%) occurred mainly caused by the changing refractive-index characteristics. This finding is in agreement with calculations by *Ackermann* [1998]. During INDOEX, the relative humidity was mostly between 40% and 80% and the impact of the relative humidity on the lidar ratio was found to be small (compare section 4.3). Thus we conclude that a significant increase of the lidar ratio is only possible if the ratio of the particle absorption to the scattering coefficient or/and the particle size distribution changes significantly.

[51] The remaining parameters in Figure 8 to be discussed are the Ångström exponents. As mentioned, these values were mostly calculated from backscatter coefficients at 400, 532, and 800 nm (after equation (2)), which were available only at heights above 1000 m because of overlap problems (compare section 3). As can be seen, the mean Ångström exponents for the short wavelengths decreased with increasing cluster number (1 to 4). The exponents ranged mostly from 1 to 1.6 for Southeast Asian particles, from 0.8 to 1.4 for North Indian pollution, and from 0.6 to 1 for South Indian air masses. A weak opposite trend, i.e., an increasing Ångström exponent from clusters 1–3, was found in the long-wavelength region. However, this trend is rather uncertain because of large uncertainties of 20–40% of the individual values. A significant change of the Ångström exponents with height was not observed. Obviously the particle size characteristics were almost the same throughout the lofted haze layers. As expected, the marine values were low ($\leq$0.5, cluster 4).

[52] The relationship between the Ångström exponents and the observed air masses above 1000-m height is further investigated in Figure 11. The underlying map of the ratio of aerosol emission fluxes originating from fossil fuel combustion and biomass combustion in India is determined from emission inventory data [*Reddy and Venkataraman*, 2002a, 2002b] in the way described by *Venkataraman et al.* [1999] and *Reddy and Venkataraman* [2000]. In the northern and central eastern parts of India (cluster-1 region) and along the east coast of southern India large areas with a rather low ratio of fossil fuel combustion to biomass combustion (dark blue in Figure 11) exist. With a few exceptions, mainly in the northwestern, western, and southernmost parts of India (including hot-spot-like urban areas with ratios >5) the fossil-fuel/biomass aerosol burden ratio is <1 in India.

[53] In Figure 11, 21 out of 26 of the trajectories for very low Ångström exponents <1 (short-wavelength range) indicated that the air mass originated from India. For high Ångström exponents >1.5, the majority (11 out of 15) of the trajectories indicated an airflow from Southeast Asia (and eastern Asia). The main reason for the comparably low Indian Ångström exponents is believed to be the high contribution of biomass combustion (fuelwood, crop waste, dung cake) to the aerosol formation. A feature specific to Indian aerosols is that biofuel combustion particles are larger (0.5–1-μm diameter) than diesel combustion particles (0.1–0.5-μm diameter) [*Venkataraman and Rao*, 2001].

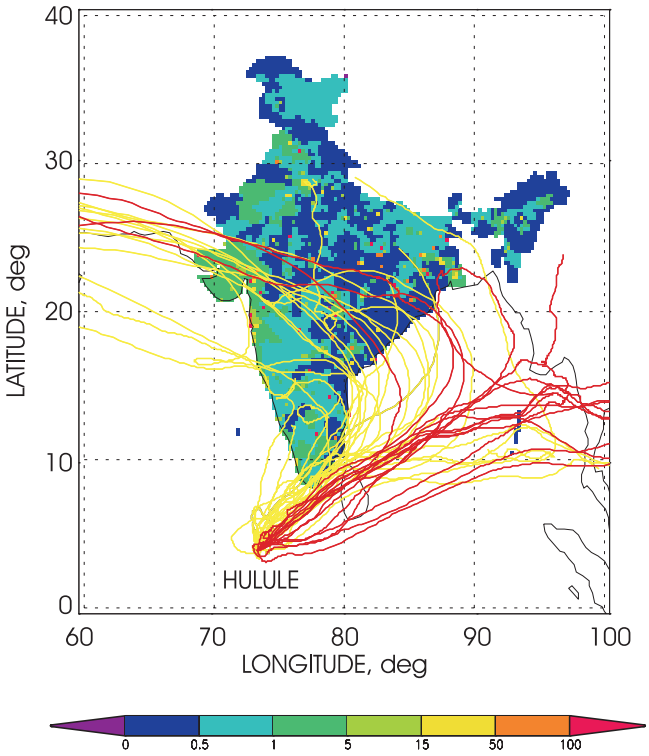

Figure 11. Geographical distribution of the ratio of the aerosol loading caused by fossil fuel combustion to the one caused by biomass combustion (underlying map, mainly in blue and green) for the INDOEX IFP period, backward trajectories (in red) for lofted aerosols showing a high Ångström exponent for short wavelengths of >1.5 (indicating a relatively small mean particle radius), and backward trajectories (in yellow) for low Ångström exponents <1 (indicating a relatively large mean particle radius).

Therefore, Indian plumes are likely to contain larger particles, on average, than the European, North American, or East Asian plumes. This behavior is in agreement with Figure 11. According to *Streets and Waldhoff* [1998] biomass combustion contributes about 25% to the total fuel consumption in Thailand, 34% in the Philippines, 25% in China, and <1% in Japan.

[54] In Figure 12, Indian (clusters 2 and 3) and European (ACE 2) Ångström exponents [*Ansmann et al.*, 2002] are compared. The Indian values are clearly shifted toward lower Ångström exponents. The pronounced peak at 0.8–1 for Indian aerosols is caused by cluster-3 values. Values similar to the ACE-2 data were found for the Southeast Asia cluster (not shown).

[55] In the discussion of possible reasons for the comparably low Ångström values for Indian aerosols several other reasons have to be taken into account as already mentioned in section 4.1. Long-range transport of coarse-mode soil particles from the Arabian Peninsula or semiarid and desert regions in India as well as road dust (highest contribution during the dry northeast monsoon season) could lead to a reduction of the Ångström exponents, especially in the long-wavelength region. However, the influence of dust appears to be generally small according to our observations of the depolarization ratio. The depolarization ratio is defined here as the ratio of the particle backscatter coefficients determined from the perpendicular and parallel components of the lidar return signals at 710 nm with respect to the transmitted, linearly polarized light. In the case of significant backscattering by desert and road dust arriving from India the respective depolarization ratio should be significantly different from the depolarization ratio found in Southeast Asian aerosols. However, our depolarization ratios were mostly below 5% even in Indian haze and were thus at all in the range typical for anthropogenic aerosols [*Ferrare et al.*, 2001; *Murayama et al.*, 1999].

[56] Aging of the aerosol particles is believed to lead to a significant shift of the accumulation mode toward larger sizes and to a respective decrease of the Ångström values. Reasons are mainly condensation and liquid-phase chemical reactions. This effect certainly had an impact on the INDOEX Ångström values as a whole. It remains unclear in which way differences in the aging of biomass burning aerosols and fossil fuel particles influenced the results.

[57] Furthermore, the number of fires is highest in India and Indochina in March [*Goloub and Arino*, 2000]. Forest fires may also lead to an increase of the number of larger particles. *Wandinger et al.* [2002] found large effective radii of about 0.25 μm or a corresponding count median diameter (CMD) of the accumulation mode of 0.3 μm and rather low Ångström values (close to zero) in forest fire plumes that had traveled from Northwest Canada to Europe within six days. *Reid et al.* [1998] reported CMD values of about 0.21 μm for aged particles originating from rain forest fires

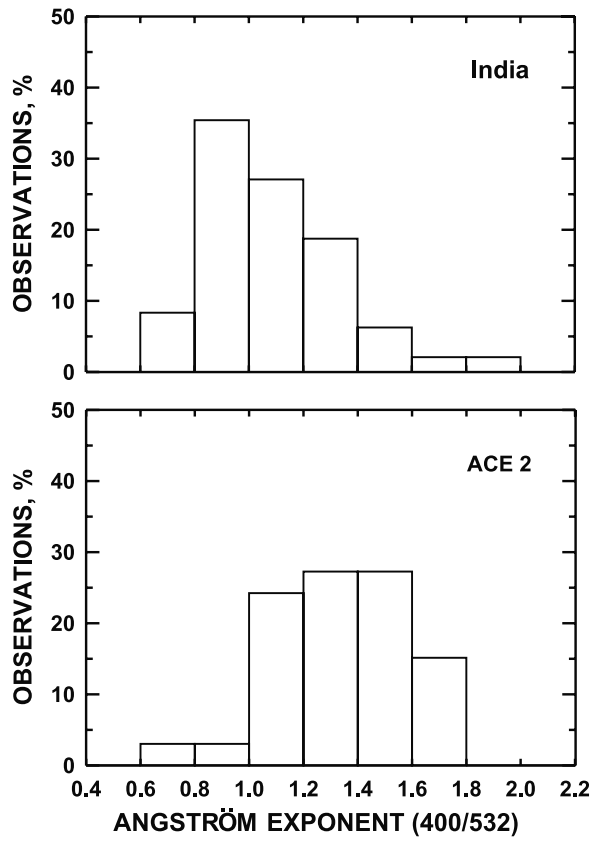

Figure 12. Distribution of the Ångström exponents for the short wavelengths for India (clusters 2 and 3) and for ACE 2 (European pollution outbreaks).

in Brazil. *Radke et al.* [1988] found CMD values of about 0.22 μm near forest fires in North America and a tendency that particles grow with age.

[58] A comprehensive data set of Ångström exponents is also available from the KCO Sun photometer observations. *Eck et al.* [2001] frequently measured Ångström exponents from 1.1–1.5 (for the 440–870 nm spectrum) during INDOEX even in cases with moderate particle optical depth of 0.2–0.4 at 440 nm (0.15–0.35 at 500 nm). However, simple calculations with a variable impact of marine particles show that Sun photometer observations do not allow a precise determination of the pollution-related Ångström exponents because of the unknown influence of marine particles. If we assume a contribution of marine particles close to 0.1 to the total particle optical depth and an Ångström exponent of 0.2 for the marine particles (as we concluded from our combined lidar/photometer observations during INDOEX IFP [*Wagner et al.*, 2001] and the October-1999 observations), the Ångström exponents for the anthropogenic particles are 2.9–4.1, 1.7–2.4, and 1.5–2 for measured particle optical depths of 0.15, 0.25, and 0.35, respectively (in the case of the measured column Ångström exponents of 1.1–1.5). By assuming a marine particle optical depth of 0.05 instead of 0.1, as found by *Welton et al.* [2002] over the Indian Ocean south of the equator, the respective pollution-related Ångström exponents are about 50%, 30%, and 20% lower for the respective optical depths of 0.15, 0.25, and 0.35. In any case of the marine particle influence, the KCO Sun-photometer-derived Ångström exponents are larger than the lidar values for the lofted pollution plumes and significantly larger than the respective Hulule Sun photometer values for 532-nm particle optical depths of 0.15–0.35 [*Wagner et al.*, 2001]. The reason for these differences between the KCO and Hulule observations is not clear and may in part be caused by the fact that KCO is closer to India (source region, higher fraction of small particles, lower impact of marine particles on the optical depth).

[59] *Léon et al.* [2001] measured particle optical depth spectra at Goa at the west coast of southern India and at another urban site about 100 km east of Goa. They used the same type of photometer as employed at KCO and found Ångström exponents (from the wavelength pair 440/670 nm) mostly from 1.4–1.6. Here, local influences (new particle formation and a reduced impact of aging effects) and the absence of marine particles have to be considered in the data interpretation.

4.3. Correlation Analysis

[60] A correlation analysis was performed to investigate the relationships between the particle extinction coefficient at 532 nm, the lidar ratio, and the Ångström exponents and the dependence of the optical properties on relative humidity. In Figure 13, the relationship between the extinction coefficient and the lidar ratio for the lowermost layer (<1000-m height) and for the free-tropospheric layers from 1000–2500-m height are shown, separately for the defined three clusters. For comparison, clean marine values measured in October 1999 (cluster 4) are included in Figure 13a. A clear correlation is found for the lowermost 1000 m during the northeast monsoon season. An increase of the lidar ratio with increasing extinction coefficient indicates

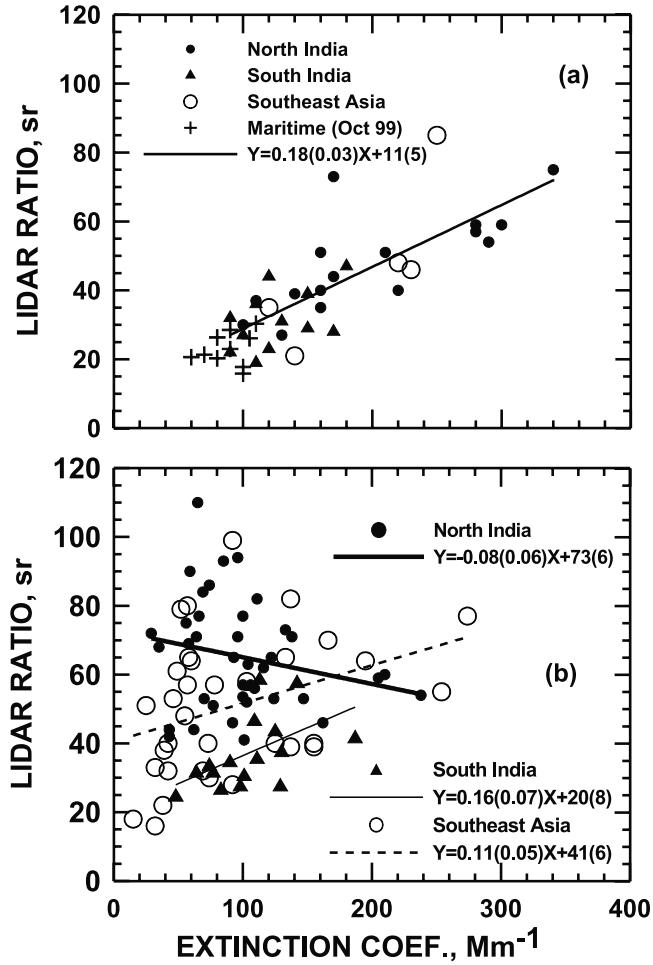

Figure 13. (a) Relationship between the column-mean extinction coefficient at 532 nm and the column-mean lidar ratio for the lowermost layer (<1000-m height). (b) Lidar ratio versus extinction coefficient in the lofted layers. Values for clusters 1–4 are indicated by different symbols. Lines show linear fits including all data (Figure 13a). In Figure 13b the lines are calculated separately for clusters 1–3. The respective fit parameters (standard deviation in parentheses) are given in the plots. The correlation coefficients are 0.77 for Figure 13a and 0.35 (Southeast Asia), −0.22 (North India), and 0.58 (South India) for Figure 13b.

the increasing impact of anthropogenic particles on light extinction or, vice versa, a decreasing influence of marine particles on total light scattering.

[61] The correlation between the particle extinction coefficient and the lidar ratio in the pollution layers in the free troposphere is weak (compare Figure 13b). The complex behavior reflects the rather large range of the continental particle characteristics. Another reason for the weak correlation in Figure 13b is the fact that the extinction coefficient (extensive aerosol state parameter) is indicative for the particle amount which typically decreases with height. In contrast the lidar ratio (intensive aerosol state parameter) is indicative for the internal aerosol properties and it was often found to be roughly independent of height.

[62] In Figure 14, the Ångström exponents for the short and long wavelengths are plotted versus the extinction

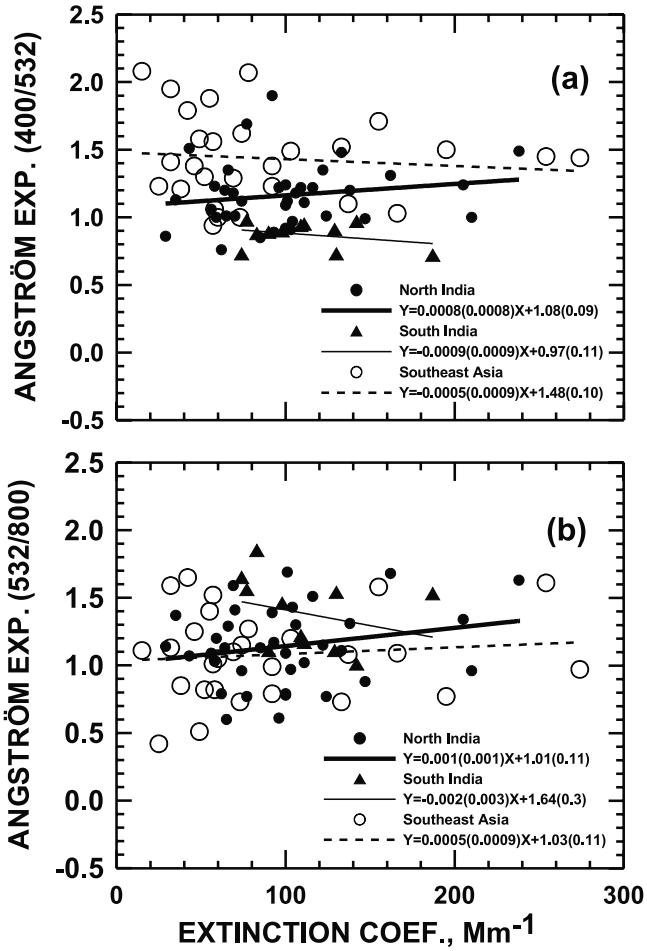

Figure 14. Relationship between the 532-nm particle extinction coefficient and (a) the Ångström exponent for short wavelengths and (b) the Ångström exponent for long wavelengths. Symbols, lines, and fit parameters for each cluster are explained in the plots. The correlation coefficients are −0.1 (Southeast Asia), 0.17 (North India), and −0.3 (South India) for Figure 14a and 0.1 (Southeast Asia), 0.22 (North India), and −0.29 (South India) for Figure 14b.

coefficient at 532 nm in the lofted plumes. The uncorrelated behavior between the two quantities implies that the characteristics of the size distribution is independent of the strength of the aerosol loading. The same behavior was observed during ACE 2 at the Portuguese coast [*Ansmann et al.*, 2002].

[63] Based on KCO Sun photometer observations during INDOEX, *Eck et al.* [2001] found a strongly decreasing Ångström exponent (340–440-nm spectrum) with increasing optical depth. They argued that the correlation indicates a shift of the accumulation mode toward larger sizes with increasing pollution optical depth (column-integrated extinction coefficient). However, a correlation between the Ångström exponent considering all wavelengths from 440–870 nm and the optical depth was not found.

[64] In Figure 15, the Ångström exponents are plotted versus the lidar ratio. Again, a clear trend is not visible. According to Mie-scattering calculations the lidar ratio decreases with increasing effective radius (associated with decreasing Ångström exponents). The opposite effect is observed here. This finding may again underline the dominant effect of light absorption on the lidar ratio. As mentioned above, low Ångström exponents may indicate biomass combustion aerosols (large fraction of larger particles) which, on the other hand, contain a comparably high amount of BC particles.

[65] Figure 16a shows the correlation between the extinction coefficient and the relative humidity in the aerosol layers above 1000-m height. According to the regression lines in Figure 16a, the extinction coefficient increased by factors of 1.8 (Southeast Asia) and 2.5 (South India) when the relative humidity increased from 30% to 80%. No relationship between relative humidity and extinction coefficient was found for the North India cluster. For the ACE-2 pollution plumes, the particle extinction coefficient increased by a factor of 2.2 when the humidity increased from 30% to 80%. Respective mean factors of 2.3 and 2.0 were found in polluted air off the mid-Atlantic coast of the United States [*Kotchenruther et al.*, 1999] and in polluted

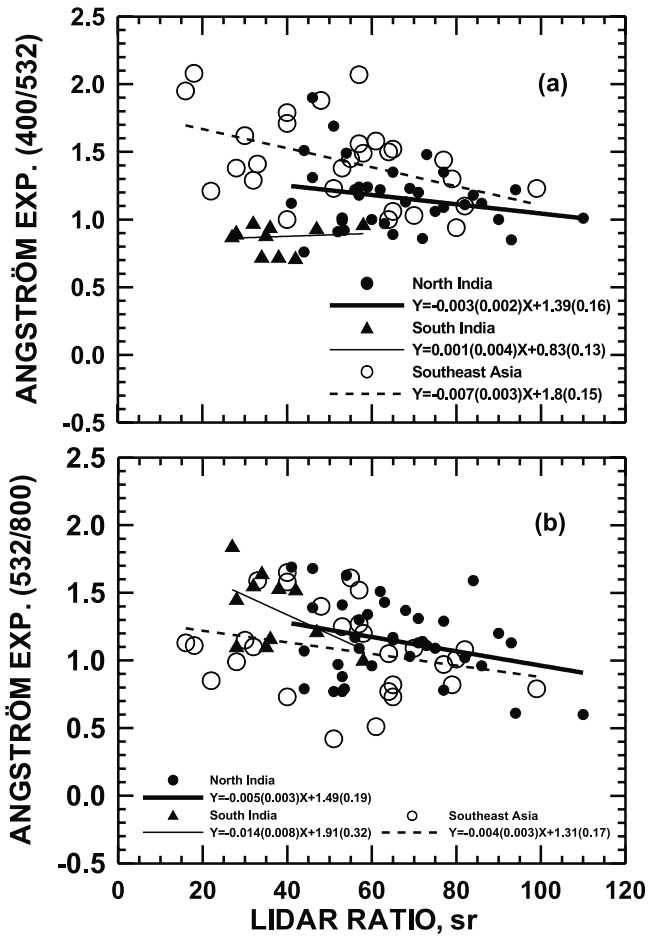

Figure 15. Relationship between the 532-nm lidar ratio and (a) the Ångström exponent for short wavelengths and (b) the Ångström exponent for long wavelengths in the lofted aerosol layers. Symbols, lines, and fit parameters are indicated in the plots. The correlation coefficients are −0.46 (Southeast Asia), −0.24 (North India), and 0.1 (South India) for Figure 15a and −0.28 (Southeast Asia), −0.3 (North India), and −0.49 (South India) for Figure 15b.

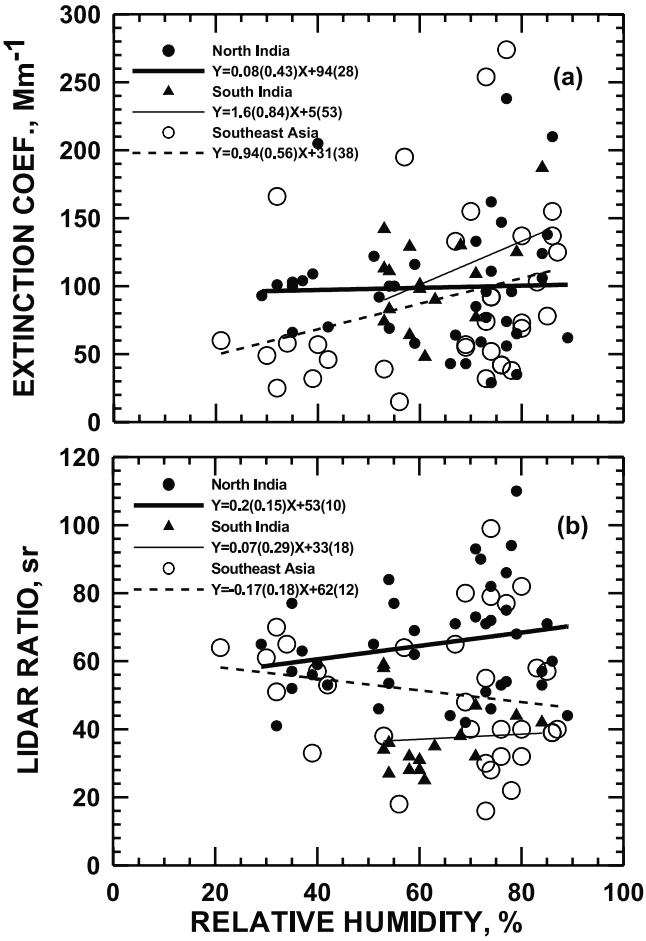

Figure 16. (a) The 532-nm particle extinction coefficient versus relative humidity and (b) lidar ratio versus relative humidity for the clusters 1–3. Lines show the linear fits. The respective fit parameters are given in addition. The correlation coefficients are 0.29 (Southeast Asia), 0.03 (North India), and 0.45 (South India) for Figure 16a and −0.17 (Southeast Asia), 0.22 (North India), and 0.07 (South India) for Figure 16b.

marine air in the region around the Canary Islands during ACE 2 [*Gassó et al.*, 2000].

[66] Figure 16b, finally, shows the correlation between the lidar ratio and the relative humidity in the lofted plumes. According to model calculations of *Ackermann* [1998] the extinction coefficient of a given anthropogenic particle population increases much more with increasing humidity than the 180° backscatter coefficient. As a consequence, the lidar ratio was found to increase by about 15% when the relative humidity increased from 30% to 80%. Observations by *Ferrare et al.* [2001] in Oklahoma were in good agreement with these model calculations. The South India data show a similar behavior. In the case of the Southeast Asia cluster the lidar ratio decreased with increasing relative humidity because of a stronger increase of the backscatter coefficient with relative humidity compared to the respective increase of the extinction coefficient.

[67] An increase of the lidar ratio by approximately 15% was also found for the North India cluster (compare Figure 16a). However, this was caused by the fact that the backscatter coefficient decreased with increasing relative humidity by about 15%. The behavior of both the extinction coefficient and the backscatter coefficient for northern Indian aerosols may be interpreted as a hint that a large fraction of these particles was not only highly absorbing but also hydrophobic. It is interesting to note that *Kotchenruther and Hobbs* [1998] found a similar behavior for biomass burning aerosols in Brazil. The scattering coefficient increased by a factor of 1.0–1.5 (mean value 1.16) when the relative humidity increased from 30% to 80%. We found respective changes of the extinction coefficients of 1.04 ± 0.16 in Indian aerosols. In agreement with our results concerning particle backscattering, they observed a decrease of the aerosol backscatter ratio by 10–20% when the humidity increased from 30% to 80%. The backscatter ratio is defined here as the ratio of the hemispheric backscattering to total scattering.

[68] For completeness, it remains to be mentioned that a relationship between the Ångström exponent and relative humidity was not found. The correlation coefficients were all below 0.35, and changes of the Ångström values with increasing relative humidity (from 30% to 80%) were of the order of ±2%. This behavior is consistent with the fact that Ångström exponents are formed from extinction ratios so that the humidity growth effect widely cancels out.

5. Conclusions

[69] A complex aerosol lidar was deployed in the tropics. The six-wavelength lidar allowed us to determine vertical profiles of optical properties of Indo-Asian haze layers under ambient conditions. Heavily polluted conditions were observed over the Maldives, more than 3000 km south of the main anthropogenic sources. Volume extinction coefficients of the particles at 532 nm typically ranged from 25–175 Mm^{-1} in the elevated haze layers in the free troposphere. Particle optical depths of up to 0.7 at 532 nm were measured. The pollution above 1000 m contributed 30–60% to the total particle optical depth at Hulule. Lidar ratios were frequently >70 sr. By means of backward trajectories, emission data for India, and the lidar-ratio data, northern Indian aerosols were identified to be highly absorbing. The comparably low Ångström exponents indicated that the aged, anthropogenic aerosol particles from India were larger than aerosol particles measured, e.g., in aged European or Southeast Asian pollution plumes.

[70] Because of the observed high extinction values, the Indo-Asian haze clearly has a strong impact on regional climate. However, because the particles were in part highly absorbing, possibly hydrophobic, and were often found above the boundary layer so that the aerosol layers could be transported over thousands of kilometers without significant removal, the impact is certainly much more complex than the picture delivered by present-day global atmospheric models [see, e.g., *Ramanathan et al.*, 2001b].

[71] This contribution was also intended to demonstrate the need for advanced lidar observations, especially in environments with complex aerosol layering. It is increasingly recognized that global maps of aerosol optical depths in combination with a qualitative knowledge about the aerosol composition (refractive index characteristics) are not sufficient to quantify the impact of aerosols on the physical (and chemical) processes in the atmosphere. Vertically resolved

aerosol measurements (on a regional and global scale) are required to improve our knowledge about aerosol layering, the causes for this layering, and the related consequences.

[72] **Acknowledgments.** We highly appreciate the generous support by the Government of the Maldives, particularly by Abdullahi Majeed, the Deputy Minister of Home Affairs, Housing, and Environment. We furthermore extend our appreciation to the staff of the Maldives Meteorological Office and to the Maldives Airport Authority for their logistic support. We are grateful to H. Hube of IFT for experimental support and the authors' institutes for supporting the data analysis.

References

Ackerman, A. S., O. B. Toon, D. E. Stevens, A. J. Heymsfield, V. Ramanathan, and E. J. Welton, Reduction of tropical cloudiness by soot, *Science*, *288*, 1042–1047, 2000.

Ackermann, J., The extinction-to-backscatter ratio of tropospheric aerosol: A numerical study, *J. Atmos. Oceanic Technol.*, *15*, 1043–1050, 1998.

Althausen, D., D. Müller, A. Ansmann, U. Wandinger, H. Hube, E. Clauder, and S. Zörner, Scanning six-wavelength eleven-channel aerosol lidar, *J. Atmos. Oceanic Technol.*, *17*, 1469–1482, 2000.

Angevine, W. M., M. T. Trainer, S. A. McKeen, and C. M. Berkowitz, Mesoscale meteorology of the New England coast, Gulf of Maine, and Nova Scotia: Overview, *J. Geophys. Res.*, *101*, 28,893–28,901, 1996.

Ångström, A., Techniques for determining the turbidity of the atmosphere, *Tellus*, *13*, 214–223, 1961.

Ansmann, A., M. Riebesell, and C. Weitkamp, Measurement of atmospheric aerosol extinction profiles with a Raman lidar, *Opt. Lett.*, *15*, 746–748, 1990.

Ansmann, A., M. Riebesell, U. Wandinger, C. Weitkamp, E. Voss, W. Lahmann, and W. Michaelis, Combined Raman elastic-backscatter lidar for vertical profiling of moisture, aerosol extinction, backscatter, and lidar ratio, *Appl. Phys. B*, *55*, 18–28, 1992.

Ansmann, A., D. Althausen, U. Wandinger, K. Franke, D. Müller, F. Wagner, and J. Heintzenberg, Vertical profiling of the Indian aerosol plume with six-wavelength lidar during INDOEX: A first case study, *Geophys. Res. Lett.*, *27*, 963–966, 2000.

Ansmann, A., F. Wagner, D. Althausen, D. Müller, A. Herber, and U. Wandinger, European pollution outbreaks during ACE 2: Lofted aerosol plumes observed with Raman lidar at the Portuguese Coast, *J. Geophys. Res.*, *106*, 20,725–20,734, 2001.

Ansmann, A., F. Wagner, D. Müller, D. Althausen, A. Herber, W. von Hoyningen-Huene, and U. Wandinger, European pollution outbreaks during ACE 2: Optical particle properties from multiwavelength lidar and star/Sun photometry, *J. Geophys. Res.*, *107*(D15), 4259, doi:10.1029/2001JD001109, 2002.

Collins, W. D., P. J. Rasch, B. E. Eaton, B. V. Khattatov, J.-F. Lamarque, and C. S. Zender, Simulating aerosols using a chemical transport model with assimilations of satellite aerosol retrievals: Methodology for INDOEX, *J. Geophys. Res.*, *106*, 7313–7336, 2001.

Cooney, J. A., J. Orr, and C. Tomasetti, Measurements separating the gaseous and aerosol components of laser atmospheric backscatter, *Nature*, *224*, 1098–1099, 1969.

Crutzen, P. J., and V. Ramanathan, Foreword, *J. Geophys. Res.*, *106*, 28,369–28,370, 2001.

Eck, T. F., B. N. Holben, O. Dubovik, A. Smirnov, I. Slutsker, J. M. Lobert, and V. Ramanathan, Column-integrated aerosol optical properties over the Maldives during the northeast monsoon for 1998–2000, *J. Geophys. Res.*, *106*, 28,555–28,566, 2001.

Fernald, F. G., Analysis of atmospheric lidar observations: Some comments, *Appl. Opt.*, *23*, 652–653, 1984.

Ferrare, R. A., S. H. Melfi, D. N. Whiteman, K. D. Evans, R. Leifer, and Y. J. Kaufman, Raman lidar measurements of aerosol extinction and backscattering, 1, Methods and comparisons, *J. Geophys. Res.*, *103*, 19,663–19,672, 1998.

Ferrare, R. A., D. D. Turner, L. Heilman Brasseur, W. F. Feltz, O. Dubovik, and T. P. Tooman, Raman lidar measurements of the aerosol extinction-to-backscatter ratio over the Southern Great Plains, *J. Geophys. Res.*, *106*, 20,333–20,347, 2001.

Franke, K., Optische und physikalische Eigenschaften süd- und südostasiatischer Aerosolpartikel: Beobachtungen mit einem Sechswellenlängenlidar auf den Malediven während INDOEX, Ph.D. thesis, 100 pp., Inst. for Tropospheric Res., Leipzig, Germany, 2003.

Franke, K., A. Ansmann, D. Müller, D. Althausen, F. Wagner, and R. Scheele, One-year observations of particle lidar ratio over the tropical Indian Ocean with Raman lidar, *Geophys. Res. Lett.*, *28*, 4559–4562, 2001.

Gassó, S., et al., Influence of humidity on the aerosol scattering coefficient and its effect on the upwelling radiance during ACE 2, *Tellus, Ser. B*, *52*, 546–567, 2000.

Goloub, P., and O. Arino, Verification of the consistency of POLDER aerosol index over land with ATSR-2 fire product, *Geophys. Res. Lett.*, *27*, 899–902, 2000.

Haywood, J. M., and K. P. Shine, Multi-spectral calculations of the direct radiative forcing of the tropospheric sulphate and soot aerosols using a column model, *Q. J. R. Meteorol. Soc.*, *123*, 1907–1930, 1997.

Heintzenberg, J., and A. Mészáros, Elemental carbon, sulfur and metals in aerosol samples at a Hungarian regional air pollution station, *Időjárás*, *89*, 313–319, 1985.

Klett, J. D., Stable analytical solution for processing lidar returns, *Appl. Opt.*, *20*, 211–220, 1981.

Kotchenruther, R. A., and P. V. Hobbs, Humidification factors of aerosols from biomass burning in Brazil, *J. Geophys. Res.*, *103*, 32,081–32,089, 1998.

Kotchenruther, R. A., P. V. Hobbs, and D. A. Hegg, Humidification factors for atmospheric aerosols off the mid-Atlantic coast of the United States, *J. Geophys. Res.*, *104*, 2239–2251, 1999.

Léon, J.-F., et al., Large-scale advection of continental aerosols during INDOEX, *J. Geophys. Res.*, *106*, 28,427–28,439, 2001.

Masonis, S. J., K. Franke, A. Ansmann, D. Müller, D. Althausen, J. A. Ogren, A. Jefferson, and P. J. Sheridan, An intercomparison of aerosol light extinction and 180° backscatter as derived using in-situ instruments and Raman lidar during the INDOEX field campaign, *J. Geophys. Res.*, *107*(D19), 8014, doi:10.1029/2000JD000035, 2002.

Mattis, I., A. Ansmann, D. Müller, U. Wandinger, and D. Althausen, Dual-wavelength Raman lidar observations of the extinction-to-backscatter ratio of Saharan dust, *Geophys. Res. Lett.*, *29*(9), 1306, doi:10.1029/2002GL014721, 2002.

Melfi, S. H., Remote measurements of the atmosphere using Raman scattering, *Appl. Opt.*, *11*, 1605–1610, 1972.

Melfi, S. H., J. D. Lawrence, and M. P. McCormick, Observation of Raman scattering by water vapor in the atmosphere, *Appl. Phys. Lett.*, *15*, 295–297, 1969.

Müller, D., U. Wandinger, and A. Ansmann, Microphysical particle parameters from extinction and backscatter lidar data by inversion with regularization: Theory, *Appl. Opt.*, *38*, 2346–2357, 1999.

Müller, D., F. Wagner, D. Althausen, U. Wandinger, and A. Ansmann, Physical properties of the Indian aerosol plume derived from six-wavelength lidar observations on 25 March 1999 of the Indian Ocean Experiment, *Geophys. Res. Lett.*, *27*, 1403–1406, 2000.

Müller, D., K. Franke, F. Wagner, D. Althausen, A. Ansmann, and J. Heintzenberg, Vertical profiling of optical and physical particle properties over the tropical Indian Ocean with six-wavelength lidar, 1, Seasonal cycle, *J. Geophys. Res.*, *106*, 28,567–28,575, 2001a.

Müller, D., K. Franke, F. Wagner, D. Althausen, A. Ansmann, J. Heintzenberg, and G. Verver, Vertical profiling of optical and physical particle properties over the tropical Indian Ocean with six-wavelength lidar, 2, Case studies, *J. Geophys. Res.*, *106*, 28,577–28,595, 2001b.

Murayama, T., H. Okamoto, N. Kaneyasu, H. Kamataki, and K. Miura, Application of lidar depolarization measurement in the atmospheric boundary layer: Effects of dust and sea-salt particles, *J. Geophys. Res.*, *104*, 31,781–31,792, 1999.

Neusüß, C., et al., Characterization and parameterization of atmospheric particle number-, mass-, and chemical-size distributions in central Europe during LACE 98 and MINT, *J. Geophys. Res.*, *107*(D21), 8127, doi:10.1029/2001JD000514, 2002.

Novakov, T., T. S. Bates, and P. K. Quinn, Shipboard measurements of concentrations and properties of carbonaceous aerosols during ACE-2, *Tellus, Ser. B*, *52*, 228–238, 2000a.

Novakov, T., M. O. Andreae, R. Gariel, T. W. Kirchstetter, O. L. Mayol-Bracero, and V. Ramanathan, Origin of carbonaceous aerosols over the tropical Indian Ocean: Biomass burning or fossil fuels?, *Geophys. Res. Lett.*, *27*, 4061–4064, 2000b.

Pelon, J., C. Flamant, P. Chazette, J.-F. Léon, D. Tanré, M. Sicard, and S. K. Satheesh, Characterization of aerosol spatial distribution and optical properties over the Indian Ocean from airborne lidar and radiometry during INDOEX'99, *J. Geophys. Res.*, *107*(D19), 8029, doi:10.1029/2001JD000402, 2002.

Podgorny, I. A., and V. Ramanathan, A modeling study of the direct effect of aerosols over the tropical Indian Ocean, *J. Geophys. Res.*, *106*, 24,097–24,105, 2001.

Quijano, A. L., I. N. Sokolik, and O. B. Toon, Radiative heating rates and direct radiative forcing by mineral dust in cloudy atmospheric conditions, *J. Geophys. Res.*, *105*, 12,207–12,219, 2000a.

Quijano, A. L., I. N. Sokolik, and O. B. Toon, Influence of the aerosol vertical distribution on the retrievals of aerosol optical depth from satellite radiance measurements, *Geophys. Res. Lett.*, *27*, 3457–3460, 2000b.

Radke, L. F., D. A. Heggs, J. H. Lyons, C. A. Brook, P. V. Hobbs, R. Weiss, and R. Rasmussen, Airborne measurements on smoke from biomass burning, in Aerosols and Climate, edited by P. V. Hobbs and M. P. McCormick, pp. 411–422, A. Deepak, Hampton, Va., 1988.

Ramanathan, V., et al., Indian Ocean Experiment: An integrated analysis of the climate forcing and effects of the great Indo-Asian haze, *J. Geophys. Res.*, *106*, 28,371–28,398, 2001a.

Ramanathan, V., P. J. Crutzen, J. T. Kiehl, and D. Rosenfeld, Aerosols, climate, and the hydrological cycle, *Science*, *294*, 2119–2124, 2001b.

Rasch, P. J., W. D. Collins, and B. E. Eaton, Understanding the Indian Ocean Experiment (INDOEX) aerosol distributions with an aerosol assimilation, *J. Geophys. Res.*, *106*, 7337–7355, 2001.

Reddy, M. S., and C. Venkataraman, Atmospheric optical and radiative effects of anthropogenic aerosol constituents from India, *Atmos. Environ.*, *34*, 4511–4523, 2000.

Reddy, M. S., and C. Venkataraman, Inventory of aerosol and sulphur dioxide emissions from India, part I, Fossil fuel combustion, *Atmos. Environ.*, *36*, 677–697, 2002a.

Reddy, M. S., and C. Venkataraman, Inventory of aerosol and sulphur dioxide emissions from India, part II, Biomass combustion, *Atmos. Environ.*, *36*, 699–712, 2002b.

Reid, J. S., P. V. Hobbs, R. J. Ferek, D. R. Blake, J. V. Martins, M. R. Dunlap, and C. Liousse, Physical, chemical, and optical properties of regional haze dominated by smoke in Brazil, *J. Geophys. Res.*, *103*, 32,059–32,080, 1998.

Reid, J. S., T. F. Eck, S. A. Christopher, P. V. Hobbs, and B. N. Holben, Use of the Ångström exponent to estimate the variability of optical and physical properties of aging smoke particles in Brazil, *J. Geophys. Res.*, *104*, 27,473–27,489, 1999.

Sasano, Y., E. V. Browell, and S. Ismail, Error caused by using a constant extinction/backscatter ratio in the lidar solution, *Appl. Opt.*, *24*, 3929–3932, 1985.

Scheele, M., P. Sigmund, and P. van Velthoven, Sensitivity of trajectories to data resolution and its dependence on the starting point: In or outside the tropopause fold, *Meteorol. Appl.*, *3*, 267–273, 1996.

Streets, D. G., and S. T. Waldhoff, Biofuel use in Asia and acidifying emissions, *Energy*, *23*, 1029–1042, 1998.

Venkataraman, C., and G. U. M. Rao, Emission factors of carbon monoxide and size-resolved aerosols from biofuel combustion, *Environ. Sci. Technol.*, *35*, 2100–2107, 2001.

Venkataraman, C., B. Chandramouli, and A. Patwardhan, Anthropogenic sulphate aerosol from India, estimates of burden and direct radiative forcing, *Atmos. Environ.*, *33*, 3225–3235, 1999.

Wagner, F., D. Müller, and A. Ansmann, Comparison of the radiative impact of aerosols derived from vertically resolved (lidar) and vertically integrated (Sun photometer) measurements: Example of an Indian aerosol plume, *J. Geophys. Res.*, *106*, 22,861–22,870, 2001.

Wandinger, U., and A. Ansmann, Experimental determination of the lidar overlap profile with Raman lidar, *Appl. Opt.*, *41*, 511–514, 2002.

Wandinger, U., et al., Optical and microphysical characterization of biomass-burning and industrial-pollution aerosols from multiwavelength lidar and aircraft measurements, *J. Geophys. Res.*, *107*(D21), 8125, doi:10.1029/2000JD000202, 2002.

Welton, E. J., K. J. Voss, P. K. Quinn, P. J. Flatau, K. Markowicz, J. R. Campbell, J. D. Spinhirne, H. R. Gordon, and J. E. Johnson, Measurements of aerosol vertical profiles and optical properties during INDOEX 1999 using micropulse lidars, *J. Geophys. Res.*, *107*(D19), 8019, doi:10.1029/2000JD000038, 2002.

D. Althausen, A. Ansmann, K. Franke, and D. Müller, Institute for Tropospheric Research, Permoserstrasse 15, 04318 Leipzig, Germany. (dietrich@tropos.de; albert@tropos.de; franke@tropos.de; detlef@tropos.de)

M. S. Reddy, Laboratoire d'Optique Atmosphérique, Centre National de la Recherche Scientifique, Université des Sciences et Technologies de Lille 1, 59655 Villeneuve d'Ascq, France. (reddy@loaser.univ-lille1.fr)

R. Scheele, Koninklijk Nederlands Meteorologisch Instituut, P. O. Box 201, 3730 AEDe Bilt, Netherlands. (scheele@knmi.nl)

C. Venkataraman, Centre for Environmental Science and Engineering, Indian Institute of Technology, Bombay, Powai, Mumbai 400 076, India. (chandra@cc.iitb.ac.in)

F. Wagner, Meteorological Institute, University of Munich, Theresienstrasse 37, 80333 München, Germany. (fwagner@meteo.physik.uni-muenchen.de)